Assessment and control of organic and other contaminants associated with the Stardust sample return from comet 81P/Wild 2

Scott A. SANDFORD[1*], Saša BAJT[2], Simon J. CLEMETT[3], George D. CODY[4], George COOPER[5],
Bradley T. DEGREGORIO[6], Vanessa DE VERA[7], Jason P. DWORKIN[8], Jamie E. ELSILA[8],
George J. FLYNN[9], Daniel P. GLAVIN[8], Antonio LANZIROTTI[10], Thomas LIMERO[7],
Mildred P. MARTIN[8,11], Christopher J. SNEAD[12], Maegan K. SPENCER[13], Thomas STEPHAN[14],
Andrew WESTPHAL[15], Sue WIRICK[16], Richard N. ZARE[17], and Michael E. ZOLENSKY[18]

[1]NASA-Ames Research Center, Astrophysics Branch, Mail Stop 245-6, Moffett Field, California 94035–1000, USA
[2]Institute of Geophysics and Planetary Physics, Lawrence Livermore National Laboratory, Livermore, California 94550, USA
#Present address: DESY Deutsches Elektronen-Synchrotron, Notkestraße 85, 22607 Hamburg, Germany
[3]ERC, Inc./NASA-Johnson Space Center, Houston, Texas 77058, USA
[4]Geophysical Laboratory, Carnegie Institution of Washington, Washington, D.C. 20015, USA
[5]NASA-Ames Research Center, Astrobiology Branch, Mail Stop 239-4, Moffett Field, California 94035–1000, USA
[6]Naval Research Lab., Code 6366, 4555 Overlook Ave. SW, Washington, D.C. 20375–5320, USA
[7]Wyle Integrated Science and Engineering, Houston, Texas 77058, USA
[8]Goddard Center for Astrobiology, NASA-Goddard Space Flight Center, Greenbelt, Maryland 20771, USA
[9]Physics Department, SUNY Plattsburgh, 101 Broad Street, Plattsburgh, New York 12901, USA
[10]CARS, University of Chicago, Chicago, Illinois 60637, USA
[11]The Catholic University of America, Washington, D.C. 20064, USA
[12]Department of Earth and Space Sciences, UCLA, California 90095–1567, USA
[13]Department of Chemistry, Stanford University, Stanford, California 94305–5080, USA
Present address: Sawtooth Labs, Inc., Redwood City, California 94063, USA
[14]Department of the Geophysical Sciences, The University of Chicago, 5734 South Ellis Avenue, Chicago, Illinois 60637, USA
[15]Space Sciences Laboratory, University of California at Berkeley, Berkeley, California 94720, USA
[16]Physics and Astronomy Department, SUNY at Stony Brook, Stony Brook, New York 11794–3800, USA
[17]Department of Chemistry, Stanford University, Stanford, California 94305–5080, USA
[18]1KT, NASA-Johnson Space Center, Houston, Texas 77058, USA
[*]Corresponding author. E-mail: scott.a.sandford@nasa.gov

Abstract–Numerous potential sources of organic contaminants could have greatly complicated the interpretation of the organic portions of the samples returned from comet 81P/Wild 2 by the Stardust spacecraft. Measures were taken to control and assess potential organic (and other) contaminants during the design, construction, and flight of the spacecraft, and during and after recovery of the sample return capsule. Studies of controls and the returned samples suggest that many of these potential sources did not contribute any significant material to the collectors. In particular, contamination from soils at the recovery site and materials associated with the ablation of the heatshield do not appear to be significant problems. The largest source of concern is associated with the C present in the original aerogel. The relative abundance of this carbon can vary between aerogel tiles and even within individual tiles. This C was fortunately not distributed among a complex mixture of organics, but was instead largely present in a few simple forms (mostly as $Si-CH_3$ groups). In most cases, the signature of returned cometary organics can be readily distinguished from contaminants through their different compositions, nonterrestrial isotopic ratios, and/or association with other cometary materials. However, some conversion of the carbon indigenous to the flight aerogel appears to have happened during particle impact, and some open issues remain regarding how this C may be processed into new forms during the hypervelocity impact collection of the comet dust.

INTRODUCTION

One of the scientific goals of the Stardust comet sample return mission was to establish whether cometary dust contained complex organic materials, and if so, to establish the abundance, chemical, and isotopic nature of the organic phase(s) (Brownlee et al. 2003; Tsou et al. 2003). Such information would provide key insights into the formation and evolution of the comet, and the nature of the organic material can potentially be used to place constraints on the environments and chemical processes by which the organics were originally made and subsequently evolved (e.g., Cronin et al. 1988; Bernstein et al. 1999; Sandford et al. 2000, 2001; Pizzarello et al. 2006). Characterization of any organic phases also allows an additional means by which the returned cometary materials can be compared to those seen in other extraterrestrial materials, particularly in meteorites and interplanetary dust particles (IDPs), and to the various organic materials detected in interstellar space.

In addition, it has been suggested that comets and their dust may have played an important role in delivering complex organic materials to early planetary surfaces and that these materials may have played key roles in the formation of life on Earth (e.g., Oro 1961; Oro et al. 1980; Chyba and Sagan 1992; Huebner and Boice 1992; Chyba and McDonald 1995). Insofar as our planetary system formed by universal processes, a better understanding of the delivery of organic materials to planets in our solar system by cometary dust also provides some assessment of the role such materials might play in other forming planetary systems.

The study of organic materials in extraterrestrial samples is fraught with difficulty, however. We live on a planet that is rich with life, and organic compounds are everywhere around us. Thus, organic analysis of extraterrestrial samples must deal with the potential for the presence of contaminants that may be mistakenly identified as having an extraterrestrial origin. In the case of the samples returned from comet 81P/Wild 2, this problem is exacerbated by the extremely small sizes of the returned samples (typically nanograms or less) and their intimate association with aerogel collector material, which contained some indigenous carbon.

In the paper that follows, we describe the results of a study made by members of the Stardust organics preliminary examination team (PET) to characterize the populations of potential Stardust contaminants and assess the nature of any organic contaminants found within the Stardust sampling system.

EXPERIMENTAL TECHNIQUES

During the course of the organics preliminary examination (PE), and the preparations leading up to it, the Organics PET made use of a wide variety of analytical techniques (see supporting online material [SOM] for more details). These techniques included Fourier infrared (IR) microspectroscopy, nuclear magnetic resonance (NMR) spectroscopy, luminescence imaging, liquid chromatography with UV fluorescence detection and time-of-flight mass spectrometry (LC-FD/TOF-MS), time-of-flight secondary ion mass spectrometry (TOF-SIMS), X-ray absorption near-edge spectroscopy (XANES), X-ray diffraction, and microprobe laser-desorption laser-ionization mass spectrometry ($\mu L^2 MS$). Details of these techniques and the equipment and procedures used for these analyses are summarized in the paper's SOM.

PREFLIGHT, FLIGHT, AND POSTFLIGHT CONTROLS

It was recognized from the very beginnings of the Stardust mission that special care was needed to minimize the potential exposure of the Stardust sample collection system to outside organics. Members of the science team (SS and MZ) worked with the contractor that built the spacecraft, Lockheed-Martin, during the design and construction phase of the mission to do what could be done within the resources available to maintain as clean a sampling environment as possible. Of course, it was not possible to make and maintain a *completely* contamination-free spacecraft and sampling system, and a parallel effort was also made to assess any possible contaminants that might ultimately be present in the sampling system. This effort involved the inventory and collection of samples of spacecraft construction materials that could potentially contaminate the collectors. "Witness coupons" were also used during construction, test, and flight that could be examined to assess any accumulated contaminants. During recovery of the sample return capsule (SRC) in Utah, samples were also obtained from potential contamination reservoirs, including local soil and air samples, portions of the thermal protection system, and the contents of the sample canister's air filter. Finally, considerable efforts were made to characterize the intrinsic organic contents of the aerogel tiles in which the cometary samples were collected, since these materials are in intimate contact with the majority of the returned samples.

Much of the discussion that follows involves studies of these various control samples. It should be noted

that, during the duration of the mission, samples of all these materials have been archived by the Stardust Curator at Johson Space Center (JSC) and, just as are the Wild 2 samples collected by Stardust, these materials are available for investigators to request for scientific purposes.

In the text that follows we will sequentially discuss (i) the organics associated with the Stardust aerogel collector medium, (ii) potential contaminants that could have been acquired from the Stardust spacecraft during flight, and (iii) potential contaminants from flight, re-entry, and recovery of the SRC. We then end with a discussion of relevant "lessons learned" from the flight of the Stardust mission.

ORGANICS ASSOCIATED WITH THE AEROGEL COLLECTOR MEDIUM

As noted earlier, one of the largest concerns with regard to organic contamination of the Wild 2 samples is associated with the presence of carbon in the original aerogel collector tiles. Aerogel tiles used in the Stardust collector tray were produced from tetraethyl-ortho-silicate (TEOS) using the basic process developed by Tillotson and colleagues (see Tillotson and Hrubesh 1992). However, these processes were modified in order to produce tiles with density gradients (Tsou et al. 2003; Jones 2007). The aerogel manufacturing process involved the use of TEOS, ethanol, water, nitric acid, ammonium hydroxide, and acetonitrile. In addition, a silicone based mold release was sprayed into the aerogel tile molds to prevent aerogel from adhering to the molds. After wet gel precursors were placed into the molds and allowed to form wet gels, samples were dried by high temperature supercritical solvent extraction. Finally, the cells were all baked at 350 °C to further remove volatiles and carbon. The final aerogel density gradients were measured using the Gladstone method, i.e., by measuring the deflection of a laser beam as it traversed the corner of an aerogel block to determine the index of refraction, which was then correlated to density (Jones 2007).

Aerogel tiles were made in batches from a single aerogel percursor and individual cells were selected from these batches for installation in the Stardust collector trays. Cells from 10 different batches were placed in the cometary collector tray and cells from 19 different batches were placed in the interstellar collector tray. Unused cells were collected by the Stardust Curator at JSC and samples of these preflight aerogel tiles are available for request for study.

Ideally, the aerogel manufacture process would produce aerogel that consists solely of Si and O. However, infrared measurements of early Stardust aerogel prototypes showed the original aerogel to contain significant amounts of aliphatic $-CH_3$ and $-CH_2-$ groups (S. A. Sandford, unpublished results). It was determined that this carbon was not soluble but was instead largely bonded into the aerogel network and that its abundance could be greatly decreased by heating. Stardust cells were heated to 350 °C for several hours to minimize this organic contamination. Higher heatings were not used since they removed relatively little additional carbon and could result in changes of the structure and transparency of the aerogel.

Since it was known that the flown aerogel collector tiles contained some intrinsic carbon, a number of different analytical techniques were used prior to return of the Wild 2 samples and during the PE period to address the state, abundance, and distribution of the carbon originally in the tiles. Additional work was also done to examine how this carbon can be altered during the course of hypervelocity impact by an incoming particle. The results of these efforts are described in the following sections.

The State of the Carbon in the Original Stardust Aerogel Collector Tiles

The nature of the original carbon in various Stardust aerogel tiles was examined using IR, NMR, luminescence imaging, LC-FD/TOF-MS, XANES, and $\mu L^2 MS$ analytical techniques. These studies include results obtained both from flown aerogel tiles and from materials taken from archival aerogel tiles taken from the same production batches as those flown.

Infrared Spectroscopy

Carbon originally in the aerogel can be detected in infrared (IR) transmission spectra, where absorption features in the 3050–2800/cm (3.28–3.57 μm) range characteristic of C-H stretching vibrations of aliphatic $-CH_2-$ and $-CH_3$ groups are seen. Infrared spectra demonstrated that heating of the aerogel after its production greatly decreased the abundance of, but did not fully eliminate, this material.

Numerous IR measurements were made from both Stardust flight aerogel and archival samples of unflown tiles taken from the same production batches to assess the chemical nature and distribution of this indigenous carbon in the Stardust flight aerogel tiles. For example, the results of analyses of two keystones extracted from Stardust cometary aerogel cell C2115 are shown in Figs. 1 and 2. The keystones were made using the standard techniques of Westphal et al. (2004) and were each approximately 200 to 300 μm thick. The keystones each contained the separate comet particle tracks C2115,22,20 and C2115,23,21. Both tracks showed a
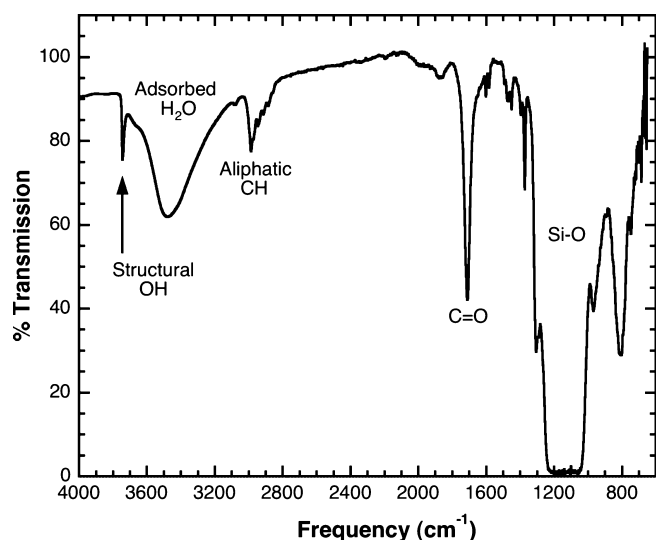
Fig. 1. Infrared spectrum of an approximately 10 μm × 10 μm spot on C2115,23,21, a keystone extracted from the C2115 Stardust aerogel flight cell. The strong Si-O, C＝O, aliphatic -CH$_2$- and -CH$_3$, structural –OH, and adsorbed H$_2$O absorption features were seen at all the spots examined and their presence is typical of Stardust flight aerogels.
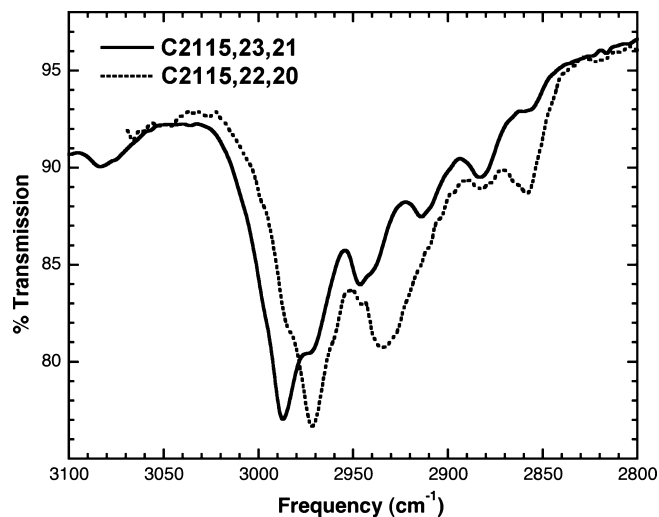

Fig. 2. Infrared spectra in the C-H stretching region taken approximately 560 μm away from the centers of tracks C2115,22,20 (dashed line) and C2115,23,21 (solid line) in their respective keystones.

fairly typical "ginseng" shape, and had comparable lengths of approximately 900 μm (see Bajt et al. 2009 for an image of track C2115,22,20). IR spectra for contamination measurements were made approximately 500 μm from each track through a square aperture 10 μm on a side.

The infrared spectra of these keystones are generally typical of Stardust aerogels and show a strong, broad Si-O stretching absorption feature near 1000 cm^{-1} (10 μm) characteristic of amorphous silicates (Fig. 1). In addition, aliphatic C-H stretching absorption features due to aliphatic -CH$_3$ and -CH$_2$- groups are seen between 3000 and 2850 cm^{-1} (3.3– 3.5 μm), C＝O stretching features are seen near 1700 cm^{-1} (5.88 μm), and "structural O-H" bands are seen near 3700 cm^{-1} (Fig. 1). Spectra typically show a broad band spanning the 3600–3200 cm^{-1} range due to H$_2$O adsorbed onto aerogel surfaces.

While the IR spectra of all Stardust aerogels show similar spectra, several issues can make it difficult to assess the full extent of aerogel contamination in the IR spectra of Stardust samples. These include variations in the amount and state of the contaminant between and within individual tiles and the presence, around some tracks, of cometary organics that were dispersed into the surrounding aerogel during impact collection (see Sandford et al. 2006; Bajt et al. 2009).

An example of variations between different pieces of aerogel can be seen in Fig. 2, which shows the aliphatic C-H features measured from the C2115,22,20 and C2115,23,21 keystones. These features show distinctly different profiles. In addition, the intensity of the -CH$_3$ feature varied by a factor of 2 to 3 from point to point in each keystone, a variation larger than expected due to likely thickness or density variations of the aerogel in the keystones. However, quantitative determination of the -CH$_3$ abundance was not possible because the Si-O absorption, which is a direct measure of the aerogel mass in the analysis beam, was saturated, making it impossible to determine the -CH$_3$/Si-O ratio.

The point-to-point variation in the IR spectra of the organic contamination in the Stardust aerogel can make quantitative background subtraction, and thus the precise determination of the infrared spectra of cometary organics, difficult. Despite these variations, the -CH$_3$ absorption was always significantly stronger than the -CH$_2$- absorption in the Stardust flight aerogel samples we analyzed. Additionally, the aliphatic component of collected Wild 2 organics has high -CH$_2$-/-CH$_3$ ratios (see Keller et al. 2006; Sandford et al. 2006; Rotundi et al. 2008; Bajt et al. 2009), which allows for IR spectral detection of cometary organic matter despite the residual aerogel carbon. Nonetheless, it is clear that comet organic matter whose spectrum is dominated by aliphatic CH$_3$ groups would be extremely difficult to positively identify, and that considerable care must be taken in the interpretation of the IR spectra of Stardust samples.

Nuclear Magnetic Resonance

Samples of aerogel tiles from several of the flight aerogel batches were analyzed using ^{1}H, ^{13}C, and ^{29}Si solid state NMR. One sample was taken from tile

E232-1A, which came from a batch noted to exhibit high luminescence under UV light (see discussion of aerogel luminescence in the next section), while another was taken from tile E235-3C, which came from a batch that showed low luminescence. Details of the NMR analytical methods used can be found in the paper's SOM.

^{29}Si Solid State NMR—Prior to discussing the NMR results, it is worth considering the synthesis chemistry behind the aerogel. The standard precursor molecules for the synthesis of aerogel include tetramethyl and/or tetraethyl orthosilicate. Condensation polymerization of these is typically performed in predominantly polar, aprotic solvents with some water added as an initiator. The degree to which the polymerization is complete, i.e., the extent to which all oxygen atoms are bonded to two silicon atoms, is readily determined via ^{29}Si NMR. This can be easily observed in the NMR spectrum of condensed silicic acid (Fig. 3), wherein a peak at approximately -113 ppm corresponds to the fully polymerized silica (Q_4, i.e., silica tetrahedra with four bridging oxygens, Si-O-Si). Weaker peaks due to partially polymerized silica tetrahedral species having one and two nonbridging oxygen species are also seen (Q_3, approximately -104 ppm, and Q_2, approximately -95 ppm, respectively). In the case of the two aerogel samples (E235-5C and E232-1A), the ^{29}Si NMR spectra are dominated by the Q_4 species, although there exists a pronounced shoulder at the characteristic frequency for Q_3 species and a hint of a shoulder at the characteristic frequency for Q_2 species (Fig. 3). Fitting of these spectra with Gaussian line shapes indicates that approximately 27% and approximately 21% of the silica tetrahedra are Q_3, in E232-1A and E235-3C, respectively, with the remainder being predominantly Q_4.

In the case of condensed silicic acid, all non-bridging oxygens are expected to be terminated by a proton ($H+$). However, in the case of the aerogel samples, the nonbridging oxygens may be terminated by un-reacted methoxy or ethoxy groups. If all Q_3 species were so terminated, this would yield a very large organic carbon background, e.g., the atomic C/Si ratio could be on the order of 0.4 for these aerogels. As we shall see later, the actual C/Si is much lower than this, suggesting that many of the aerogel Q_3 species in these aerogels may actually be terminated with protons. Furthermore, it has been shown that in aerogel, Si-O· radical defects are present and are a source of photoluminescence (Nishikawa et al. 1996), a property that Stardust aerogel tiles show to a variable degree (see next section). Indeed, as noted earlier, the fact that the low luminescence E235-3C aerogel has a lower
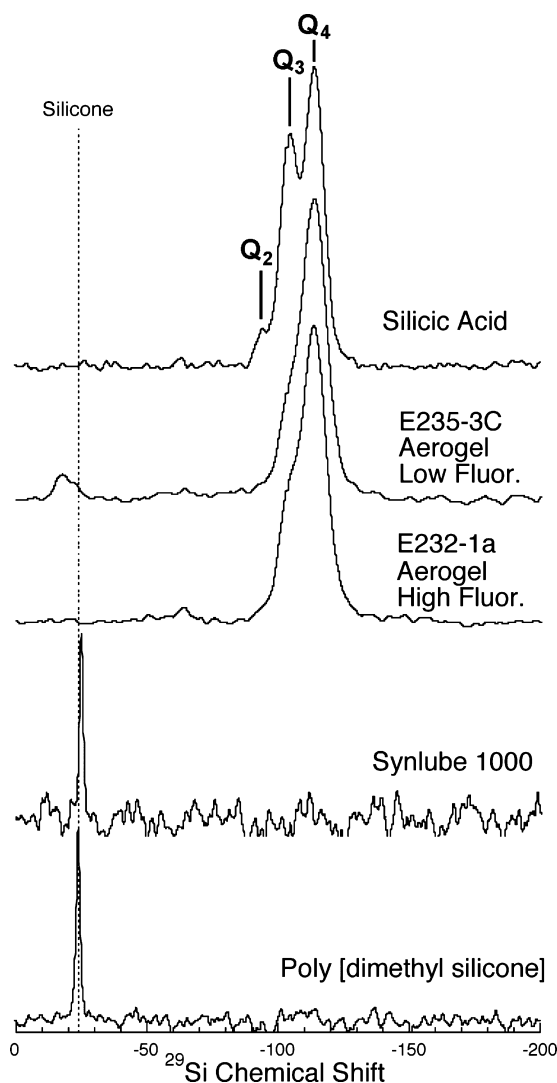

Fig. 3. ^{29}Si NMR spectra (from top to bottom) of condensed, solid, silicic acid, aerogel samples E235-3C and E232-1A, a solution of Synlube 1000 (a silicone release agent), and polymethylsilicone grease. The silicic acid solid state NMR spectrum reveals the presence of three different silicate electronic environments Q_4, Q_3, and Q_2, corresponding to 0, 1, and 2 nonbridging oxygen groups, respectively. The aerogel samples exhibit a predominance of Q_4 but with a pronounced shoulder corresponding to approximately 20–30% Q_3. In the case of the low luminescence aerogel sample, E235-3C, a minor peak at approximately -15 ppm indicates the presence of some silicone moieties.

abundance of Q_3 sites than the high luminescence E232-1A gel may support the idea that the luminescence is due to such defects. One wrinkle to this scenario, however, is that ^{29}Si in close proximity to Si-O· radicals will be unobservable due to the excessive line broadening associated with electron–nucleus dipolar interactions. However, the presence of abundant radicals can result in the need for excessive NMR probe

retuning during measurement, something we did not need to do. We therefore conclude that most of the Q_3 species in the aerogel samples are likely terminated with protons.

Finally, there is the issue of whether the Synlube 1000 used as a release agent to coat the aerogel mold surfaces to aid removal of the aerogel blocks has contributed any detectible organic matter to the aerogels that might be ultimately confused with cometary organics. In Fig. 3, a ^{29}Si spectrum of Synlube 1000 is presented along with a sample of poly[dimethyl silicone] grease. The valence of silicon in silicone is $2+$, as opposed to $4+$ for silicon in silicate. The reduction in surrounding oxygen atoms in silicone results in a large shift of characteristic resonant frequencies to distinctly higher frequencies than that of silicates, i.e., to chemical shifts of approximately -25 ppm. In Fig. 3, both Synlube 1000 and a sample of poly[dimethyl silicone] grease exhibit sharp resonances at approximately -25 ppm. Interestingly, there is clearly a small spectral feature at approximately -15 ppm in the ^{29}Si NMR spectrum of the E235-3C aerogel in the frequency range expected for silicone. While it is possible that this peak could reveal the presence of Synlube 1000 contamination, it appears more likely that these silicone moieties were actually created during aerogel synthesis. This conclusion is supported by the fact that a 10 ppm difference in frequency is quite large (in fact, too large to be ascribed to differences between Synlube 1000 methyl silicone moieties in a "neat" environment as opposed to coating aerogel). Furthermore, the peak width appears too great for a simple compound; the line width of the peak at -15 ppm is more typical of amorphous solids.

The intensity of the -15 ppm (methyl silicone) peak is approximately 6% of the total ^{29}Si NMR signal, which could imply a C/Si ratio of between 0.12 and 0.06 independent of what the presence of unreacted methoxy and ethoxy groups might add. It should be noted, however, that no attempt was made to assess the T_1 relaxation behavior of ^{29}Si in these aerogels, and it is certainly possible that ^{29}Si in the silicone moieties would relax much faster than the silicates due to the proximity to the fluctuating magnetic fields derived from the protons on the rotating methyl groups. Thus, if there were any longitudinal saturation occurring, the outcome would be an enhanced sensitivity for the methyl silicone groups. As we shall see based on the other spectroscopy, the relative abundance of methyl-silicone detected via ^{29}Si NMR appears to be about right.

^{13}C Solid State NMR—The presence of silicone methyl, methoxy, and/or ethoxy groups in aerogel can be verified directly with ^{13}C solid state NMR. Figure 4 presents CPMAS ^{13}C NMR spectra of the aerogel

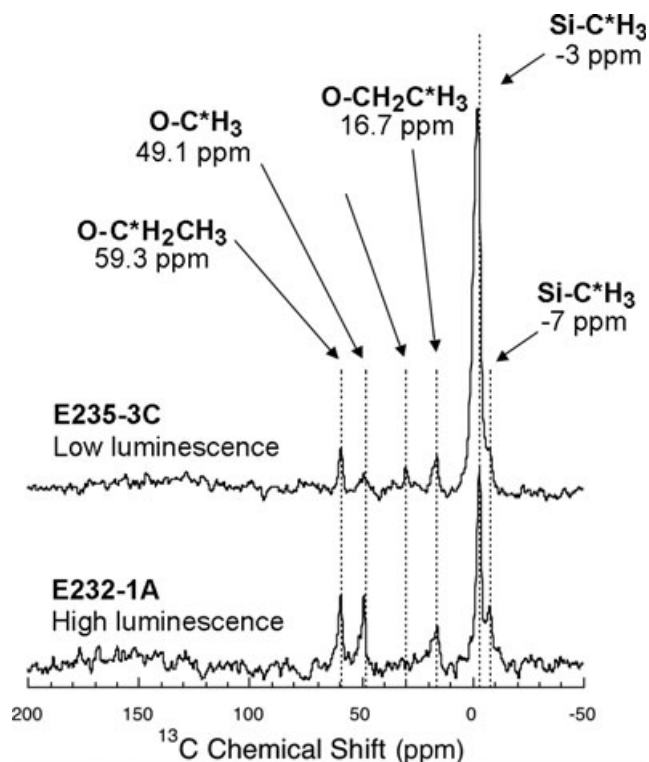Fig. 4. ^{1}H-^{13}C cross polarization solid state NMR spectra of aerogel samples from tiles E235-3C (low luminescence) and E232-1A (high luminescence). The presence of carbon corresponding to silicate bound ethoxide and methoxide, along with a more abundant methyl silicone moiety at approximately -3 and -7 ppm, is clearly revealed.

samples E235-3C and E232-1A. In both cases the most intense peak occurs at very low frequencies, -3 ppm, with a shoulder at -7 ppm, consistent with an assignment to methyl groups in silicone moieties. In addition, there are a small number of peaks that most likely correspond to silicate bound methoxy and ethoxy groups spanning the frequency range from approximately 17 ppm up to 60 ppm (Fig. 4). These peaks make it clear that there is organic carbon associated with the aerogel, and that overall the carbon chemistry is quite simple and is dominated by methyl groups.

It should be noted that the carbon signal for both aerogel samples is very weak. In order to place some constraints on actual carbon abundance in these aerogels, we can compare the signal strength per mass of sample with that of an NMR standard, e.g., hexamethylbenzene (HMB). Assuming similar cross polarization dynamics apply for both the HMB and the aerogel, the aerogels E232-1A and E235-3C carry 0.3 and 1.0 μM/mg carbon, respectively, yielding C/Si ratios of 0.02 and 0.06, respectively. These estimates constitute lower limits, i.e., if any difference in CP dynamics exists
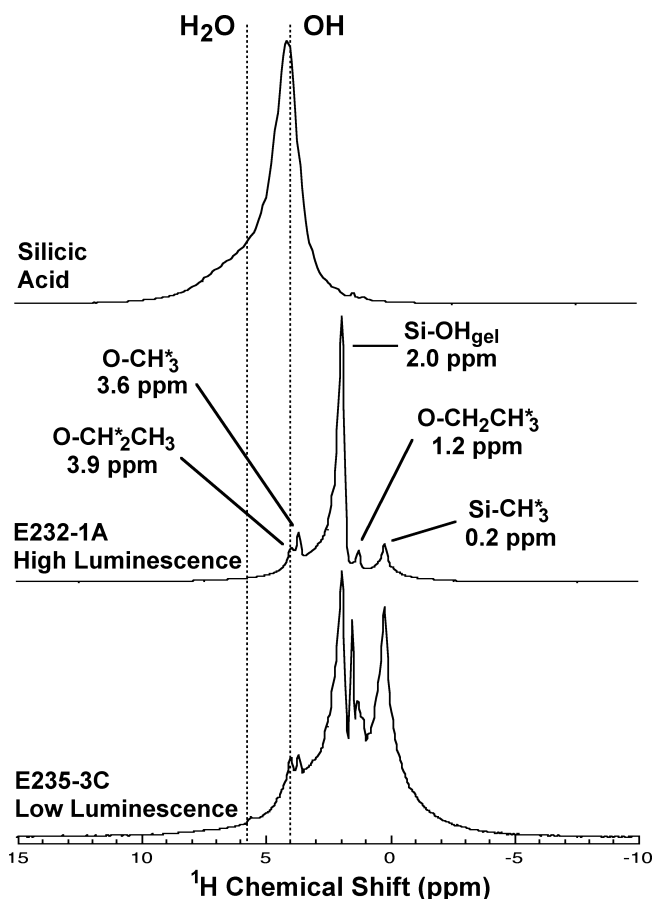
Fig. 5. ^{1}H solid state NMR spectra of silicic acid (top) and aerogel samples E232-1A (middle) and E235-3C (bottom). In addition to Si-OH and structural (nonliquid) water that contributes to the very broad peak spanning the entire frequency range, the aerogel samples reveal sharp peaks that indicate the presence of hydrogen in silicate ethoxide and methoxide functional groups, as well as silicone methyl groups.

solid through hydrogen bonding. In the case of both aerogels, the intense peak at 2 ppm is assigned to Si-OH groups. Note that the frequency shift of this peak relative to that observed in condensed silicic acid (at approximately 4 ppm) is not unusual in the case of ^{1}H NMR. The exposed ("external" to the molecular unit) nature of protons (relative to ^{13}C or [29]Si) to the environment results in frequency shifts due to even minor differences in local structure that perturb the electron current density surrounding the protons. Similar to condensed silicic acid, both aerogels exhibit a broad spectral feature that likely is closely associated H_2O. Again, the shifts in frequency of both the Si-OH and H_2O between condensed silicic acid and aerogels likely reflect differences in density and mean O-H···O distances.

As is expected on the basis of the CPMAS ^{13}C NMR spectra, the aerogel samples also exhibit ^{1}H NMR features consistent with the presence of organic carbon, e.g., protons on ethoxy, methoxy, and methyl silicone moieties (Fig. 5). The fact that the less luminescent aerogel (E235-3C) exhibits greater intensity for methyl silicone moieties than the more luminescent aerogel (E232-1A) is consistent with the ^{13}C and [29]Si spectral data. The ^{1}H data provides a link between silica species (e.g., Si-OH) and organics (e.g., CH_3) that allows us to derive an independent estimate of C/Si. Fitting the respective aerogel spectra in Fig. 5 with Gaussian band profiles and taking into consideration the relative proportion of Q_3 and Q_4 groups determined from ^{29}Si NMR (Fig. 3) reveals C/Si atomic ratios of 0.04 and 0.12, for samples E232-1A and E235-3C, respectively. These values are higher than those derived from ^{13}C NMR, but recall that the ^{13}C NMR derived estimates constitute a lower limit, and both the ^{13}C NMR data and combined ^{1}H with [29]Si data results conclude that sample E232-3C has more associated carbon.

In summary, the NMR analyses indicate that there is organic carbon in Stardust aerogels with variable C/Si ratios that are sometimes perhaps as high as 0.12. The presence of this carbon is likely an inevitable outcome of the synthesis; it is unreasonable to assume that 100% condensation of the orthosilicate precursors could actually occur. On the positive side, the NMR data reveal that this organic carbon is dominated by a few very simple functional groups, i.e., the carbon has a very simple chemistry. During particle capture, aerogel that is heated up will likely largely lose these organic functional groups through the formation of highly volatile species, e.g., methanol, ethylene, ethanol, etc. It is highly unlikely that these simple organic moieties would undergo extensive condensation reactions to form complex organic solid particles of the types described in

between HMB and the aerogel samples this would lead to an increase in the C/Si ratios inferred for the aerogels. Thus, whereas the ^{13}C NMR does directly reveal the presence of organic carbon intrinsic to the aerogel, it also reveals that this carbon is both simple in its chemistry and relatively low in abundance.

^{1}H Solid State NMR—An additional perspective on the organic carbon intrinsic to the Stardust aerogels can be obtained via ^{1}H solid state NMR, which provides a complementary (with ^{13}C and [29]Si) view of their molecular structure. Figure 5 presents the solid state ^{1}H NMR spectra of the two aerogel samples and a sample of condensed silicic acid. Condensed silicic acid produces a relatively sharp peak nearly centered on top of a broader peak—the former corresponds to Si-OH groups, the latter to structural H_2O, i.e., to nonliquid water that is strongly associated with the silicic acid
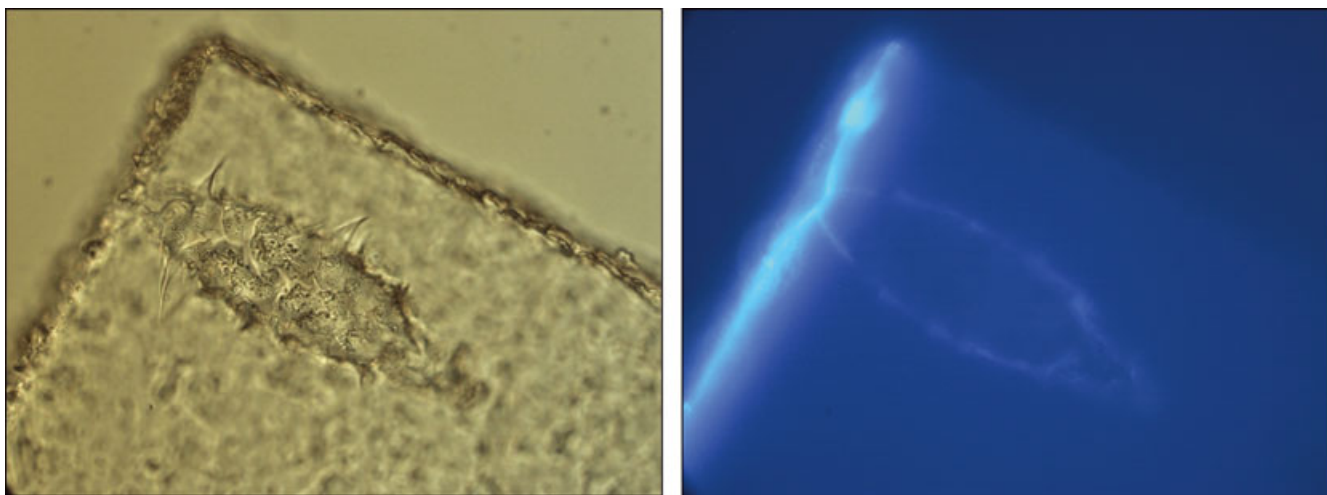
Fig. 6. Photomicrograph of Track 2 in a keystone from cometary tile C009 (left) compared with an image of the same field of view in luminescence under UV illumination (right). Note that the brightest luminescence is associated with the leftmost surface of the aerogel, which was the surface that was exposed to space.

the Stardust preliminary analyses like those reported in Sandford et al. (2006) and Cody et al. (2008). For example, one would expect such condensates to coat other materials rather than exist in discrete subgrains within larger particles. (However, as we discuss later, it is clear that a minor fraction of this carbon can be converted into dispersed, small polycyclic aromatic hydrocarbons.)

Placing a constraint on the concentration of carbon relative to silica in aerogel is also useful in establishing limits to the contribution of aerogel carbon to observed Stardust particles. Compression and, in some cases, melting of aerogel certainly occurred during particle capture, and organic-rich particles are often closely associated with compressed aerogel (cf. Cody et al. 2008). Based on these NMR data, the background C/Si (or C/O for that matter) does not exceed 0.12 (or 0.06 in the case of C/O) in Stardust aerogels. In the case of micrometer size organic particles extracted from aerogel coupons that were flown on the Stardust spacecraft, C/Si and C/O's are on the order of 1.7 and 0.6, respectively (Cody et al. 2008). This significant enrichment in carbon is difficult to explain any other way than to conclude that the additional carbon is cometary.

Luminescence

During the PE period it was noted that aerogel keystones removed from individual Stardust flight aerogel tiles showed varying degrees of visible luminescence when exposed to UV light. This was first noticed on an aerogel keystone that contained a track that had been examined by beam analysis techniques.

Several zones of luminescence were noted. Portions of the keystone that represented the space exposed surface of the aerogel tile showed the most luminescence, but increased luminescence was also seen in portions of the aerogel that had been exposed to beam analysis (Fig. 6). The presence of this luminescence raised the concern that it might be due to exposure of the surface to an organic contaminant with conjugated bonds and/or due to radiation exposure changing some of the residual carbon originally in the flight aerogel into more complex, luminescent forms.

Measurements from several keystones (both previously irradiated and unirradiated) using a fluorescent/luminescent microscope at UC Berkeley that could measure emission yield as a function of excitation wavelength failed to yield conclusive results. Different samples, and different locations in the same sample, showed essentially the same luminescence spectrum and the same energy dependence of excitation, independent of irradiation history. The biggest difference was that previously irradiated samples showed a higher overall emission intensity. These measurements were not suggestive of any particular organic compound(s) being the source of the luminescence.

To understand whether this luminescence was a more global issue on the collectors, UV illumination was then used to examine the entire collector trays at JSC. Luminescence images of the cometary collector tray were obtained using a 254 nm excitation source held at a distance of about 30 cm from the front (i.e., comet exposed) surface of the tray. A digital camera was position about 5 cm above the UV source and at a distance of about 35 cm from collector. The camera had
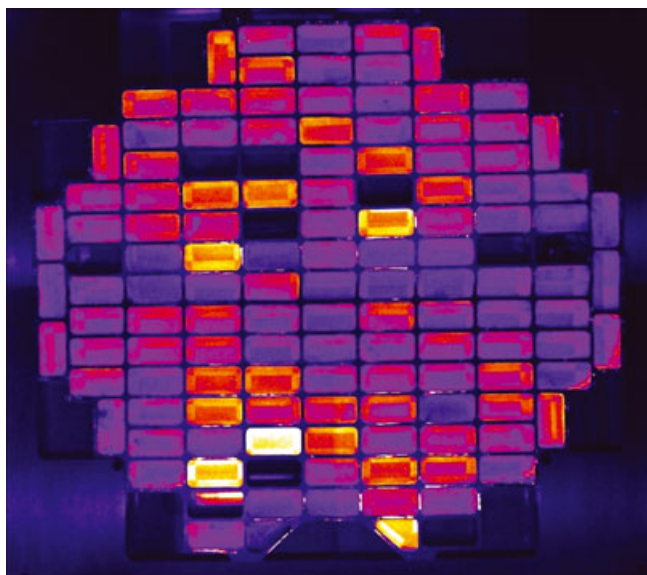
Fig. 7. Photograph of the tile luminescence in the cometary tray. Dark rectangles represent locations where tiles had already been removed for PE analysis. It is clear from these images that the luminescence is not uniformly or smoothly spread across the collector tray.

Fig. 8. A histogram plot of the rough individual tile "bulk" luminescence intensities in the aerogel tiles shown in Fig. 7. While these tiles show a smooth range of intensities, they are not random. There is a strong correlation with aerogel manufacturing batch number. Ten tiles are not shown in the plot; these include eight rectangular tiles that had already been pulled from the collector tray when the luminescence measurements were made (C009, C027, C038, C044, C054, C086, C092, and C126), and two smaller, triangular tiles near the edge of the collector (C042 and C075).

a zoom lens that was adjusted so that an individual image would cover approximately 1/4 of the collector surface. Under these conditions the imaged area had a relatively uniform UV flux. These images were then combined into composite images of the entire tray. Each image uses the green channel as a crude spectrometer, so that the intensity variations represent the luminescence emission principally in the 500–540 nm range. Each image was then processed by a de-speckling algorithm to remove CCD hot spots, corrected for lens barrel distortion, and made into a montage using an autocorrelation routine. The resultant composite image is shown in Fig. 7.

It is clear from these images that the luminescence is not uniformly or smoothly spread across the collector tray, but instead differs from tile to tile. This strongly suggests that the source of the luminescence is not a contaminant to which the entire tray has been exposed. A plot of the individual tile "bulk" luminescence intensities is shown in Fig. 8 (this information can be found in tabular form in Table S1 in the SOM). While the plot shows a smooth variation in intensities, comparison of the individual tile luminescence intensities with a map of the flight aerogel batch placement of the tiles in the tray demonstrated that the luminescence correlates strongly with production batch number. A subjective analysis of the relationship of cell luminescence with aerogel batch number in which each tile is categorized (by eye) as having low, low-medium,
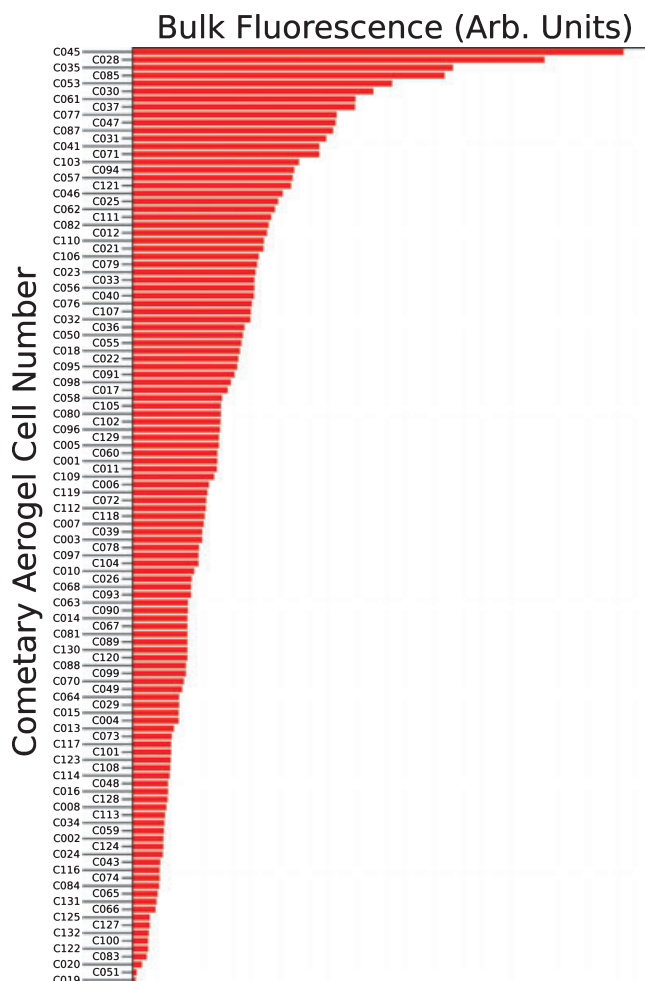
medium, medium-high, and high luminescent intensity is summarized in Table 1. It is clear that the intensity of the luminescence is batch-related, although there are a few cells that fall off the trends (see below).

Batches 227 and 232 are responsible for all the brightest cells but one. These batches contributed relatively few tiles to the tray. The tiles from these two batches are C075 (trapezoidal cell), C028, C035, C044, C085. Tile C044 (from Batch 232) was not examined because it had already been removed for other PET analysis. Batch 236 shows uniformly moderate luminescence (tiles C009 and C115, pulled for PET

Table 1. Number of cells versus intensity of luminescence.

Batch	Low	Low-med	Medium	Med-high	High	Unknown cells[a]
227	–	–	–	–	1	
232	–	–	–	–	3	044
234	14	6	1	–	–	027, 054, 086, 092
235	17	9	5	–	–	
236	–	10	15	–	–	009, 115
237	24	3	–	–	1	038, 052
239	11	1	–	–	–	126
246	1	–	–	–	–	

[a]Some cells could not be placed in the table because they had already been removed for PET analysis and were no longer available for examination for whole tile luminescence.
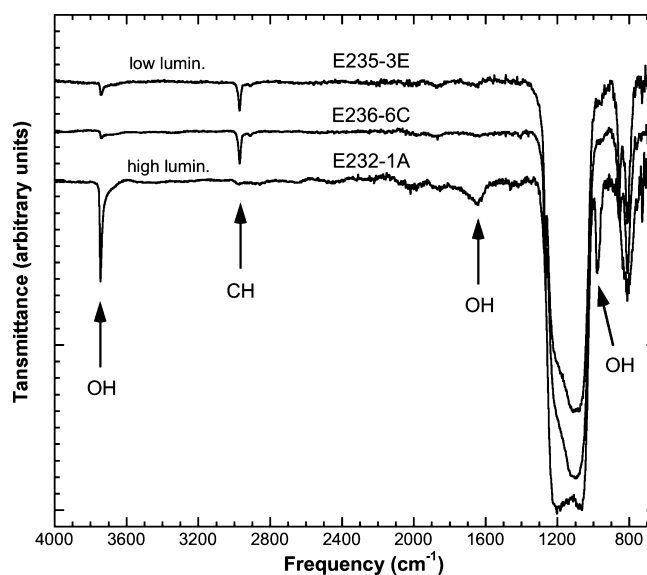

Fig. 9. Infrared absorption spectra collected from samples of aerogel tiles E235-3E (low to medium luminescence), E236-6C (low-medium to medium luminescence), and E232-1A (high luminescence). The high luminescence aerogel produces both a stronger structural –OH band near 3745 and 980 cm^{-1} and a weaker aliphatic CH band near 2970 cm^{-1}. The spectra have all been normalized to the unsaturated aerogel peak near 800 cm^{-1} peak, so variations in the strengths of the –OH and aliphatic bands are not due to difference in aerogel thickness.

analyses prior to the luminescence mapping, were in this batch). Batches 234 and 235 show generally low luminescence, but some tiles exhibit moderate luminescence. Thus, Tiles C027, C054, C086, and C092 pulled for PET analyses prior to measurement probably have low luminescence, but it could be a little higher. Batches 237, 239, and 246 consistently show very little luminescence, with the exception of tile C045, which is listed as being from Batch 237 and yet shows *very* high luminescence (the highest of all the tiles). Given the uniformity of the other cells from this batch, this suggests that tile C045 may be mislabeled. Samples from cells C038, C052, and C126, which were pulled for PET analyses prior to measurement, probably did not produce high luminescence.

The fact that adjacent cells can show greatly different luminescence intensities indicates that the source is not organics or other luminescent materials (cometary or contaminant) added after tray assembly. NMR measurements made on preflight aerogel samples (see previous section) from both a low and a high luminescence batch suggest the luminescence may be due to Q_3 defect sites, which are known to be a potential source of photo-luminescence (Nishikawa et al. 1996). The density of these sites correlates in a qualitative sense with luminescent intensity of the batches in the samples examined so far. The number of such sites might be expected to increase in aerogel exposed to ionizing radiation that could break bonds and generate new Q_3 defect sites, perhaps explaining the behavior seen in Fig. 6.

We used IR and LC-FD/TOF-MS measurements to test for any correlations between the intensity of the luminescence and the nature and abundance of organic materials detected in the aerogel tiles. IR absorption spectra taken from tiles falling in different luminescence

categories suggest that the abundance of some chemical functional groups correlate with luminescence intensity. In particular, tiles with high luminescence appear to have both considerably more structural –OH (as indicated by the bands near 3745 and 980 cm^{-1}; 2.67 and 10.2 μm) and considerably less aliphatic carbon (as indicated by the band at 2970 cm^{-1}; 3.37 μm) (Fig. 9). The structural –OH is presumably associated with locations within the aerogel in which the Si-O lattice is not completely connected and a dangling bond has been terminated with a hydrogen atom. Thus, the IR data are consistent with the NMR data—the luminescence does not correlate with the abundance of carbon in the aerogel, but seems to be more correlated with unlinked O atoms in the structure. LC-FD/TOF-MS measurements of aerogel cells from different preflight aerogel batches showed no correlation between total abundance of amines in the preflight aerogel and the intensity of the luminescence.

Overall, observations made to date suggest the luminescence in Stardust aerogel tiles is largely due to defects within the Si-O lattice. More intense luminescence at aerogel surfaces could be due to induced defects caused by solar particle irradiation. Increased luminescence induced by beam analysis techniques could also be due to production of such

Table 2. Summary of the total amine concentrations in the HCl hydrolyzed hot-water extracts of the Stardust contamination control samples analyzed during the preliminary examination period[a].

Amine detected	SRC SLA backshell (E51049)	SRC PICA heatshield (E51043)	SRC filter (5208,1,5,1,2)	UTTR mud (M4762,3)	Kapton tape (Whipple test)	Synlube 1000 (mold release)	Nylon bag (JSC curation)
D-Aspartic acid	112 ± 18	27 ± 3	< 0.1	9 ± 3	3 ± 2	< 0.1	< 0.1
L-Aspartic acid	193 ± 3	60 ± 3	< 0.1	18 ± 4	11 ± 2	< 0.1	< 0.1
D-Glutamic acid	102 ± 8	14 ± 1	< 0.1	3 ± 1	3 ± 1	< 0.1	< 0.1
L-Glutamic acid	335 ± 16	61 ± 2	< 0.1	26 ± 2	25 ± 8	< 0.1	< 0.1
D-Serine	39 ± 22	6 ± 1	< 0.1	4 ± 1	9 ± 5	< 0.1	< 0.1
L-Serine	108 ± 2	144 ± 17	1 ± 1	13 ± 1	46 ± 24	1 ± 1	< 0.3
Glycine	770 ± 109	189 ± 36	6 ± 3	45 ± 7	120 ± 16	< 0.1	3 ± 1
β-Alanine (BALA)	43 ± 1	8 ± 3	1 ± 1	4 ± 1	3 ± 1	1 ± 1	3 ± 2
γ-Amino-n-butyric acid (GABA)	127 ± 10	8 ± 1	1 ± 1	2 ± 1	8 ± 1	< 0.1	2 ± 1
D-Alanine	112 ± 24	12 ± 3	< 0.3	4 ± 1	4 ± 1	< 0.1	< 0.5
L-Alanine	310 ± 36	91 ± 13	1 ± 1	25 ± 2	13 ± 3	< 0.1	1 ± 1
D,L-β-Amino-n-butyric acid	< 0.3	< 0.1	< 0.1	< 0.1	< 0.1	< 0.1	< 0.1
α-Aminoisobutyric acid (AIB)	< 0.2	< 0.1	< 0.1	< 0.1	< 0.1	< 0.1	< 0.1
D,L-α-Amino-n-butyric acid[b]	< 0.1	< 0.1	< 0.1	< 0.1	< 0.1	< 0.1	< 0.1
D,L-Isovaline	< 0.3	< 0.5	< 0.1	< 0.1	< 0.1	< 0.1	< 0.1
ε-Amino-n-caproic acid (EACA)[c]	3,316 ± 161	3,077 ± 172	4 ± 1	2 ± 1	16 ± 1	< 0.1	176,000 ± 17,000
D-Valine	< 0.5	< 0.1	< 0.1	< 0.5	< 0.2	< 0.1	< 0.1
L-Valine	133 ± 115	24 ± 21	< 0.1	13 ± 4	11 ± 2	< 0.1	< 0.1
Methylamine (MA)	436 ± 60	4 ± 3	< 0.3	< 0.1	11 ± 1	1 ± 1	< 0.1
Ethylamine (EA)	101 ± 6	< 0.1	< 0.1	< 0.1	3 ± 1	3 ± 1	< 0.1
Ethanolamine (MEA)	74 ± 22	8 ± 5	10 ± 1	< 0.1	204 ± 60	38 ± 5	< 0.1

[a]The amine concentrations are reported as 10^{-9} mol per gram (nmol/g) on a bulk sample basis. The uncertainties ($\cdot x$) are based on the standard deviation of the average value of between two and four separate measurements (N) with a standard error, $\cdot x = \cdot x \cdot (N-1)^{-1/2}$. Upper limits are shown for amines that were not detected above procedural blank background levels.
[b]Enantiomers could not be separated under the chromatographic conditions.
[c]Major component of Nylon-6; also known as 6-aminohexanoic acid.

defects. This would also explain why the luminescence spectral properties of the "original" surface- and volume-induced luminescence look very similar. However, the origin of variable production of Si-O defects in different aerogel batches remains unclear. Nevertheless, the lack of correlation between the intensity of the luminescence and the nature and abundance of organic materials detected in the aerogel tiles using a variety of analytical techniques, suggests that organics are not primarily responsible.

LC-FD/TOF-MS Measurement of Soluble Amines in Stardust Aerogels

The LC-FD/TOF-MS analyses of soluble amines were made on preflight aerogel tiles E243-13C and E243-10F. Tile E243-13C was a preflight baked aerogel sample that had been stored under vacuum since shortly after its creation. Tile E243-10F was an unbaked aerogel sample stored in air. The results of these studies were previously reported in Glavin et al. (2008) and we only provide a brief summary of that work here. The chromatogram of Tile E243-13C shows only tiny peaks close in area to those found in the procedural blank. Trace levels of amino acids and amines were identified in these samples, including L-aspartic and L-glutamic acids, L-serine, glycine, β-alanine (BALA), γ-amino-n-butyric acid (GABA), L-alanine, ε-amino-n-caproic acid (EACA), ethanolamine (MEA), methylamine (MA), and ethylamine (EA). Total concentrations ranging from 0.04 to 3.4 nmol per gram of aerogel were found (see Table 2 of Glavin et al. 2008). No free amino acids or amines were detected in the unhydrolyzed water extract of E243-13C.

Preflight aerogel sample E243-10F had not been baked out nor stored under vacuum. It showed a similar abundance and distribution of amine compounds compared to E243-13C, with the exception that it contained much higher concentrations

(approximately 8–10×) of the amino acids GABA and EACA compared to the baked aerogel. EACA, [(NH2(CH2)5COOH)], is a monomer of the Nylon-6 polymer and has previously been shown to be a good indicator of the extent of Nylon-6 contamination of Antarctic meteorite samples during collection and storage (Glavin et al. 2006). Subsequent isotopic analysis of EACA extracted from aluminum foils that backed the aerogel cells on the Stardust collector was performed to determine its origin. The carbon isotopic ratio of the EACA was measured via gas chromatography coupled with mass spectrometry and isotope ratio mass spectrometry (GC-MS/IRMS) and compared with the carbon isotopic ratio of a piece of a storage bag used by JSC, measured by elemental analysis-isotope ratio mass spectrometry (EA-IRMS). The isotope ratios matched within experimental error ($\delta^{13}C/^{12}C$ = −25 ± 2‰ for Stardust foils, $\delta^{13}C/^{12}C$ = −26.8 ± 0.2‰ for JSC bag), implying that the EACA observed in the Stardust samples originated from the Nylon-containing bags used during curation at JSC.

ε-Amino-n-caproic acid was detected in E243-13C at much lower concentrations than in E243-10F, which is not surprising since E243-13C was stored inside a glass tube and was not directly exposed to Nylon-6 prior to analysis. No D-amino acids were detected in either preflight aerogel sample above the 0.1 nmol/g level. In addition, only trace quantities of MA and EA (0.5 to 4 nmol/g) were identified in the preflight aerogels. The ratio of MA to EA in the preflight aerogels (MA/EA approximately 7) was distinct from a ratio of approximately 1 found in the cometary exposed aerogel samples (Sandford et al. 2006; Glavin et al. 2008). Ethanolamine (MEA) was detected in both of the Stardust preflight aerogel extracts at a similar concentration. We believe that the source of the MEA contamination is most likely the mold release lubricant (Synlube 1000) used during the Stardust aerogel manufacturing process (MEA was by far the most abundant amine compound, approximately 40 nmol per gram, detected in an acid-hydrolyzed, hot water extract of Synlube 1000).

L^2MS Measurement of PAHs in Stardust Aerogels

A series of Stardust aerogel flight spare samples were analyzed using μL^{2}MS. These included 11 with layered density, six with gradient density, and 21 with mostly uniform density silica. About 16 mm^2 of each flight spare was obtained for analysis, with each sample being representative of the uppermost layer (i.e., least dense) of the installed Stardust aerogel tiles. This upper layer captured the majority of comet 81P/Wild 2 particles. Details of the sample preparation procedure can be found in the SOM. μL^{2}MS analysis of aromatic compounds in these samples showed most samples contained no measurable contamination by polycyclic aromatic hydrocarbons (PAHs). Ten of the samples, however, did exhibit distinctive, low-intensity envelopes of low-mass aromatic compounds (Spencer and Zare 2006; Spencer 2008). All samples that displayed these contaminants showed comparable and consistent patterns of m/z peaks in the μL^{2}MS mass spectra. This mass pattern included an envelope of peaks with major peaks at 135, 149, and 179 amu, which are likely 1-ring, nitrogen-containing aromatic compounds, as well as an extended series of alkylated phenanthrene. This envelope of peaks was not detected during any subsequent Stardust aerogel analyses, including in the Stardust witness coupon (see below), and was thus assigned to laboratory contamination of these nonflight aerogels incurred during storage since its synthesis in 1999. A second, distinctive envelope of peaks was also detected, including major peaks at 135, 179, 223, and 267 amu. This envelope of peaks was also seen consistently in returned Stardust aerogel samples and these masses should always be viewed with suspicion before assigning them to cometary PAHs.

STXM/XANES

Nine picokeystones of nontrack aerogel were cut from comet tray tiles and examined using both scanning transmission X-ray microscopy (STXM) and the IR microscope located at the National Synchrotron Light Source (NSLS). Seven of the picokeystones were cut from tile C2103, one picokeystone from the top (comet side) of the tile and the other six from the bottom side of the tile and two picokeystones were cut from tile C2061, both from the top of the tile. Details about the preparation and measurement of these samples can be found in the SOM. The carbon XANES spectra generally show similar features, although their relative strengths can differ substantially (Fig. 10). All the spectra contain absorption in the 285 eV region characteristic of aromatic carbon, most likely due to C = C in a ring. The breadth of this peak suggests that there generally is absorption from more than one material in this region, and in the case of trace B, the presence of two peaks shows that at least two distinct populations are present. The spectra also show absorption peaks at 288.2 eV, an energy generally assigned to C = O groups. No evidence of carbonates has been seen in these aerogel samples. Thus, the C-XANES spectra detect functional groups consistent with those seen in the aerogel using other techniques. However, these data demonstrate that the relative proportions of these groups can differ not only between tiles, but also within tiles on very small spatial scales.
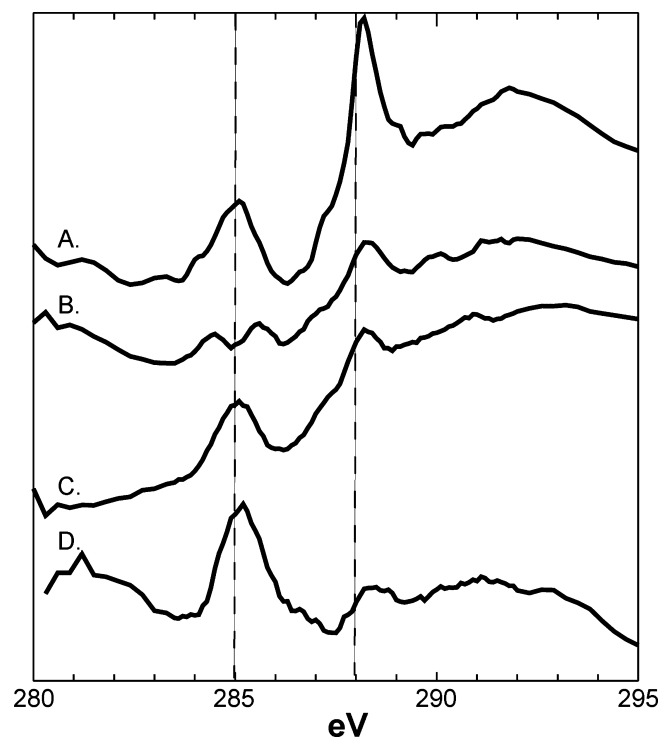
Fig. 10. Examples of the four varieties of C-XANES spectra found in nontrack containing picokeystones from Stardust flight tiles C2103 and C2061. The spectra are dominated by aromatic C=C near 285 eV and C=O near 288.2 eV, but their relative proportions can vary significantly on small size scales.

Summary of the State of the Carbon in the Original Stardust Aerogel Collector Tiles

Combined, these analyses indicate that the original Stardust aerogel collection tiles contained some "native" carbon. This carbon is not entirely uniformly distributed in the tiles and shows some compositional variation between aerogel manufacturing batches, individual tiles, and often within individual cells. Fortunately, the majority of this carbon is present in a few simple forms, primarily in methyl groups bonded in the Si-O network. However, other forms of organics were present in pre-launch aerogels, including a variety of low weight PAHs and amines.

Alteration of the Carbon Original to the Aerogel by Hypervelocity Impact

The Wild 2 particles that struck the Stardust aerogel arrived at approximately 6.1 km s^{-1}. Such collisions are sufficiently energetic that they could, depending on the specifics of kinetic energy dissipation during particle capture, alter any organic compounds originally present in both the impacting

particles and the aerogel collector material (Sandford and Brownlee 2007; Spencer and Zare 2007; Spencer et al. 2009).

The collision process of hypervelocity impacts into low porosity foams and aerogels has been modeled theoretically (Anderson and Ahrens 1994; Domínguez et al. 2004). Such models describe the general deceleration process, but do not fully describe the stochastic survival and destruction of subcomponents of complex aggregates of finer grained materials striking aerogel. It is clear from the study of the materials returned from comet 81P/Wild 2 by Stardust that some fraction of the impacting particles survived with little or no alteration, while other portions of the samples were severely heated (Brownlee et al. 2006; Flynn et al. 2006; Hörz et al. 2006; Keller et al. 2006; McKeegan et al. 2006; Sandford et al. 2006; Zolensky et al. 2006). Conversion of carbon original to the aerogel, and in the impacting cometary particles, into new forms likely occurred in a similarly variable manner. Thus, before one can assign organics seen in Stardust samples to a cometary origin, it is necessary to consider the possibility that they are either altered cometary materials or materials formed from carbon original to the aerogel.

Infrared Spectroscopy and the Survival of Aerogel Aliphatics

As noted previously, IR and NMR spectra of Stardust aerogel samples show that they contain some original carbon, most of which is in the form of aliphatic $-CH_3$ groups but a small number of other functional groups are present as well. This carbon could potentially be altered into new forms by the impact process. However, IR mapping of whole tracks in aerogel keystones suggests that this process probably does not greatly alter the chemical state of the majority of this carbon. The discovery of tracks whose IR absorption maps (typically obtained at a spatial resolution of 15 μm) show no evidence for excess absorption across the entire map indicates that the associated impacts did not produce large amounts of new materials with different chemical functionality (Sandford et al. 2006; Bajt et al. 2009). Similarly, the lack of absorption deficits in the aerogel's original absorption bands indicates that thermal conversion has not greatly depleted the original reservoir of aerogel carbon. Thus, IR spectroscopy appears to account for the majority of the original carbon, suggesting impact conversion is an inefficient process. However, IR spectroscopy is not a highly sensitive technique and the IR data do not preclude the possibility that carbon can undergo conversion at low levels (see the next section).

The Production of Small PAHs during Hypervelocity Impact

The μL^2MS technique was used in a separate study to assess the influence of hypervelocity impact on carbon contaminants in Stardust aerogel. Comet particle capture was mimicked in the laboratory using two methods, both of which utilized Stardust-type aerogel (i.e., flight spare or witness coupon aerogel) as the capture medium. The two methods were (i) hypervelocity impact of a micrometer-size borosilicate glass bead and (ii) impact simulation utilizing laser pulsed heating. Both of these studies revealed the production of a consistent, low-mass envelope of aromatic compounds (Spencer and Zare 2007; Spencer 2008; Spencer et al. 2008, 2009). Detected masses ranged from 78 to 206 amu (tentatively assigned to benzene and phenanthrene + $2CH_2$, respectively), with the most intense peak at 128 amu (naphthalene). This envelope was not detected during μL^2MS contamination control studies of the Stardust aerogel and witness coupon, as discussed elsewhere in this paper. An identical envelope of aromatic compounds was detected using μL^2MS along the dissected impact track of a Wild 2 particle in aerogel (Sandford et al. 2006). Based on these results, lightweight PAHs in samples should be viewed with suspicion as they contain a significant contribution from artifacts of the collection process, as originally suspected during the preliminary examination period (Sandford et al. 2006; Sandford and Brownlee 2007; Spencer and Zare 2007).

Summary of Impact Alteration Effects

Infrared absorption difference-maps of individual tracks suggest that impacting Stardust particles do not convert the majority of the original carbon in the aerogel tiles into new chemical forms that remain in the aerogel. However, L^2MS studies demonstrate that at least a small amount of the original aliphatic carbon in the aerogel is converted into aromatic materials in the form of lightweight PAHs. Thus, while most of the original aerogel carbon appears to be unaffected by the impact process, the issue of the possible presence of impact converted organics must be considered on a case-by-case basis whenever specific organics are being sought in Stardust aerogel samples.

POTENTIAL CONTAMINANTS FROM THE STARDUST SPACECRAFT DURING FLIGHT

There are a number of potential ways in which contaminants may have found their way into the SRC during flight. These include materials outgassed from nearby spacecraft components, propellant byproducts, and secondary materials from dust impacts on other parts of the spacecraft, particularly the Whipple shields and solar panels.

Whipple Shield and Spacecraft Materials

Cometary particles impacted on the aerogel tiles in the collector tray perpendicular to their forward surfaces. Thus, any tracks seen with oblique orientations must be either due to strikes by random interplanetary dust particles or to secondary materials from impacts on other parts of the spacecraft. Oblique tracks have, in fact, been found in the flight aerogel tiles, most of which fall in nonrandom spatial distributions on the cometary collector (Westphal et al. 2008). The materials in these tracks could include components from both the original impactor and from the spacecraft.

The source of these tracks is not entirely clear, but the preponderance of evidence points toward at least one grazing impact on the central Whipple shield of the spacecraft as the origin of clustered low-angle oblique tracks. In these tracks, the most likely contaminant would be the Mylar thermal protection material that wrapped the edge of the Whipple shields. A second population of high-angle oblique tracks unambiguously originate from a noncometary impact on the spacecraft bus just forward of the collector. The exact location of this strike on the spacecraft bus is not known, but possible contaminants include materials used for the sides of the spacecraft bus. We have used XANES to examine archived samples of these materials, which consist of a honeycomb network of aluminum foil capped by a carbon composite board attached with an adhesive glue. Small pieces of the carbon composite board and the glue were embedded in sulfur, ultramicrotomed to a thickness of 100 nm and their carbon XANES spectra were obtained. The carbon composite board consists of highly ordered graphite embedded in an epoxy matrix. Minor absorption in the graphite spectrum at 288.2 eV suggests the graphite may be slightly oxidized (Fig. 11). The carbon XANES spectra of the foil glue and the epoxy matrix indicate that both compounds are identical and differences between the carbon spectra are due to crystal orientation effects since the beam at the X1 beamline is linearly polarized. Materials in the high obliquity tracks having these spectra should be suspected of being non-cometary contaminants.

In summary, it is clear that the cometary collector tray was struck by a limited number of secondary particles resulting from impacts on other parts of the spacecraft. Materials in these oblique tracks should be viewed with considerable caution before interpreting
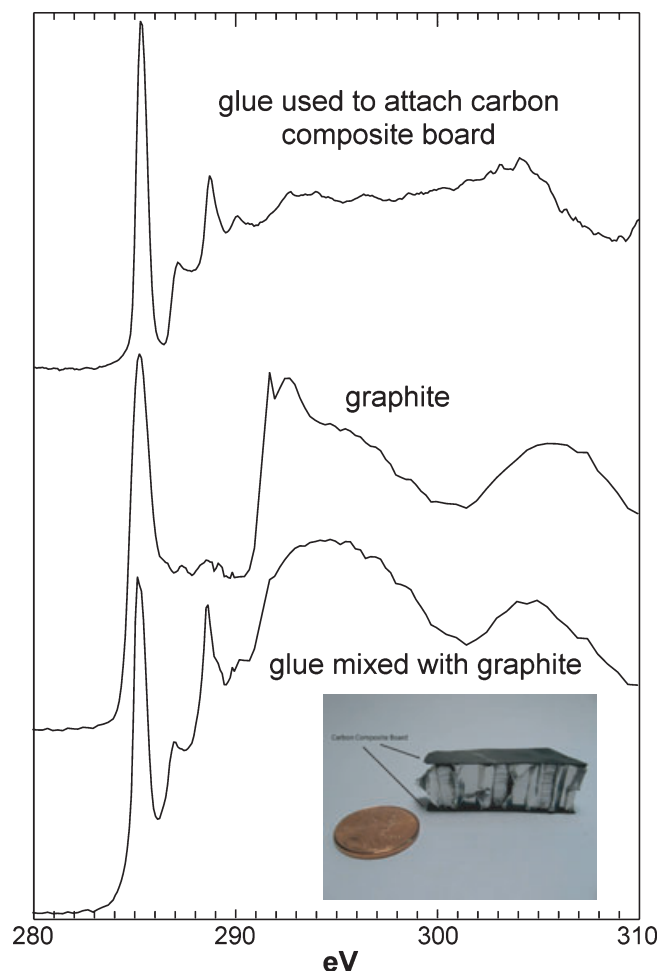
Fig. 11. Carbon XANES spectra of the glue and carbon composite board components used to make the sides of the Stardust spacecraft. The inset shows how these materials were used to surface an aluminum honeycomb structure (penny provided for scale).

their significance as possible cometary materials. Fortunately, the most likely contaminants, Mylar wrap on the Whipple shields and carbon composites from the body of the spacecraft, have distinctive C-XANES spectra that make them relatively easy to recognize. At present, there is no evidence that this process has introduced contamination outside the domain of the oblique tracks themselves.

Results of Witness Coupon Studies

It is possible that contaminants could have been introduced to the Stardust sampling trays directly from the spacecraft during its nearly 7 year flight. This is of special concern for the aerogel collectors since aerogel, with its very large surface area to mass ratio, is an excellent "sponge" for adsorbing contaminants. To

assess the extent of on-flight contamination, several "witness coupons" were enclosed in the Stardust SRC (Tsou et al. 2003). These coupons included 1 cm diameter disks of aluminum and sapphire, and one "interstellar" aerogel tile (2 cm wide × 4 cm long × 1 cm deep). These coupons were located on the arm that deployed the aerogel collector array and were placed low enough that they resided in the shadow of the main Whipple shield. Thus, these coupons were exposed to the same flight environment as the aerogel collectors for the entire mission, but were never directly exposed to the cometary influx. Samples of the aerogel witness coupon (sample WCARMI1CPN) were examined by several Organics PE Team members. The aluminum and sapphire disks have yet to be examined in detail, but showed no visible signs of adhering materials or stains. (It should be noted that none of the exposed surfaces in the Stardust sample return canister showed any signs of the "brown stain" seen on many of the surfaces of the Genesis return capsule [Hittle et al. 2006].)

LC-FD/TOF-MS and Soluble Amines

Two samples of the Stardust aerogel witness tile WCARMI1CPN (Pieces 8 and 9, 0.2 mg) were analyzed separately for amines by LC-FD/TOF-MS. Both samples of the witness tile contained the amino acids L-serine, glycine, β-alanine (BALA), γ-amino-n-butyric acid (GABA), ε-amino-n-caproic acid (EACA), and the amine ethanolamine (MEA) at levels that exceeded those found in the procedural blank. With the exception of EACA, the concentration of these amine compounds ranged from 4 to approximately 50 nmol per gram of aerogel (Glavin et al. 2008). The high concentration of predominantly bound EACA (approximately 9600 nmol/g) in the witness tile is most likely due to contamination of the aerogel with Nylon-6 polymer from the sample storage vial cap (Glavin et al. 2008). It should be emphasized that the EACA contaminant did not interfere with LC-FD/TOF-MS detection and identification of other amine compounds in any of the Stardust flight aerogel extracts. Ethanolamine (MEA) was detected in all of the Stardust preflight and flight aerogel extracts at similar relative abundances (Glavin et al. 2008). The source of MEA contamination is believed to be the Synlube 1000 mold release lubricant used during the Stardust aerogel manufacturing process (Table 2). Kapton tape also releases MEA, but significant abundances of L-serine and L-glutamic acid should have also been observed. We did not detect any D-amino acids, methylamine (MA), or ethylamine (EA) in the witness tile aerogel above the 0.2 to 8 nmol per gram level. These detection limits are approximately two orders of magnitude higher than those for the preflight aerogel samples and directly reflect the small

quantity of witness tile aerogel allocated for the PET study. In summary, the Stardust flight aerogel witness tile contains a variety of different amine contaminants that could originate from the aerogel manufacturing process, inflight spacecraft outgassing, and/or postflight storage and handling of the aerogel. However, the overall cleanliness of the witness coupon for these compounds suggests that inflight outgassing was not a dominant effect.

Laser-Desorption Laser-Ionization Mass Spectrometry

No aromatic compound contaminants were detected with $\mu L^2 MS$ when analyzing a depth profile of the Stardust witness coupon tile at normal operating parameters. At higher powers, which approximately simulated hypervelocity particle impact, a low-mass envelope of aromatic compounds was detected, as discussed earlier. These were likely (i) generated from carbon contaminants during laser pulse heating of aerogel or (ii) released from the aerogel matrix upon high-power laser desorption (Spencer and Zare 2007; Spencer 2008; Spencer et al. 2008). To eliminate the contribution from these components, all 81P/Wild 2 particle analyses were performed using a low-power desorption laser (approximately 2.5 × 10^6 W cm^{-2}).

Time-of-Flight Secondary Ion Mass Spectrometry

The aerogel witness coupon material analyzed with TOF-SIMS showed a PAH spectrum similar to that observed in a dissected aerogel keystone containing an actual cometary particle track (Stephan et al. 2008). However, compared to the witness coupon, PAH concentrations are up to a factor of six higher in aerogel associated with the track (Stephan et al. 2008). Furthermore, this factor of six may be regarded as a lower limit since the Ar^+ sputter cleaning (see SOM) that was performed on the track sample (but not on the witness coupon material) to diminish surface contamination should also have diminished the PAHs in the sample associated with the track.

IR Spectroscopy

Infrared transmission spectra were measured from a small piece of aerogel taken from the aerogel witness coupon. The background spectrum was collected the same way as for the keystones with particle tracks, i.e., by obtaining the spectrum of an "air blank" using the same optical setup as for the sample. Individual spectra from 4000 to 650 cm^{-1} were collected at about 100 μm intervals from seven different points on this piece. Each spectrum consisted of 1024 co-added scans and was collected with 4 cm^{-1} spectral resolution. Spectra of samples thin enough to avoid band saturation showed

the witness coupon was very homogenous—there was no detectible variation over a 500 μm area. Only a peak at 2970 cm^{-1}, a weak peak at 2910 cm^{-1}, and an even weaker one at 2880 cm^{-1}, corresponding to asymmetric and symmetric stretching vibrations of –CH$_3$ were detected in the C-H stretching region. Unlike many of the exposed cometary aerogels, the spectra do not contain a broad –OH peak at approximately 3300 cm^{-1} or peak associated with C=O at approximately 1700 cm^{-1}.

Summary

Analyses of the aerogel witness coupon, i.e., aerogel that was exposed to all environmental conditions as the collector aerogel *except* the comet shows similarities to collector aerogel, although the levels of contaminants, when detected, are generally lower and some components (for example, the carrier of the 1700 cm^{-1} IR C=O feature) are dramatically less abundant. This suggests that contamination associated with the operational environment of the spacecraft during flight was not a main source of contaminants associated with the samples.

POTENTIAL CONTAMINANTS FROM FLIGHT, RE-ENTRY, AND RECOVERY OF THE SAMPLE RETURN CAPSULE

Inspection of the Stardust SRC after its re-entry and recovery on January 2, 2006, indicated that it had not suffered any identifiable loss of structural integrity. Nevertheless, potential contamination must be considered since the SRC was not designed to be hermetically sealed during or after Earth return. Consequently, pressure equalization between the interior and exterior of the capsule during atmospheric re-entry provides a potential entry route into the sample canister for ablation products from the capsule's thermal protection system (i.e., the heatshield and backshell).

Due to the high velocity (12.8 km s^{-1}) associated with the hyperbolic return trajectory of the SRC, it experienced a significant heat flux during re-entry (approximately 1100W cm^{-2}), with temperatures at the stagnation point at the nose of the heatshield peaking at approximately 2700 °C. To protect the interior of the capsule during re-entry, the SRC's thermal protection system (TPS) used a phenolic impregnated carbon ablator (PICA) for the heatshield and a super light ablator (SLA 561-V) for the backshell. An ablative heatshield functions by pushing the hot shock layer of gas formed during re-entry away from the heatshield's outer surface through a process known as "blowing." Blowing occurs by the charring and pyrolysis of the outer layers of the heatshield which creates gas phase decomposition

products that then block the convective and catalytic heat flux from the underlying layers of the heatshield. Unfortunately, these same gas phase pyrolysis products also constitute a potential organic contamination threat.

In addition to potential contamination by debris sucked into the SRC during re-entry and re-pressurization, the nonhermetic seal of the SRC also allowed for the possibility of entry of atmospheric contaminants during the subsequent descent of the SRC by parachute, and soil and water samples picked up when the SRC contacted the ground.

The chief defense against the accumulation of all of these forms of potential contamination was a design that required materials entering the SRC to first pass a number of barriers before they could enter the sample canister. These barriers included backshell vents covered by meshes and a multilayer, high efficiency particulate air (HEPA) filter on the sample canister itself (Brownlee et al. 2003; Tsou et al. 2003).

In order to assess the extent to which these contaminants may have found their way into the sample canister, Organics PET members studied samples of materials from the SRC's heatshield and backshell materials (both preflight and postrecovery samples), the contents of the sample canister filter, gas samples taken during the recovery process, and samples of soils taken from the recovery site.

Heatshield and Backshell Material

As mentioned above, two different materials were used for the thermal protection system on the Stardust SRC. Phenolic Impregnated Carbon Ablator (PICA) was used for the forward heatshield and Super Light Ablator (SLA-561) was used for the backshell. The PICA consisted of a substrate of C fibers, 14–16 μm in diameter, known as Fiberform (Fiber Materials, Inc., Biddeford, ME) that was partially impregnated with the phenolic resin Durite (Bordon Packaging and Industrial Products). The SLA used for the SRC backshell consists of a highly filled elastomeric silicone material containing cork as a filler ingredient. A third material, Silicon Impregnated Reuseable Carbon Ablator (SIRCA) was considered for use on the SRC, but not ultimately used.

Carbon XANES Measurements

Carbon XANES spectral results from a preflight SLA sample show well defined absorption peaks at 285 eV, 285.35 eV, 286.6 eV, 287.4 eV, and 288.4 eV, with possible peaks at 284.4 eV and 284.6 eV suggesting a complex carbon bonding environment. XANES spectral results from a preflight PICA sample show a highly ordered graphitic material, but with additional peaks at 286.6 eV, 288.5 eV, and a possible peak at
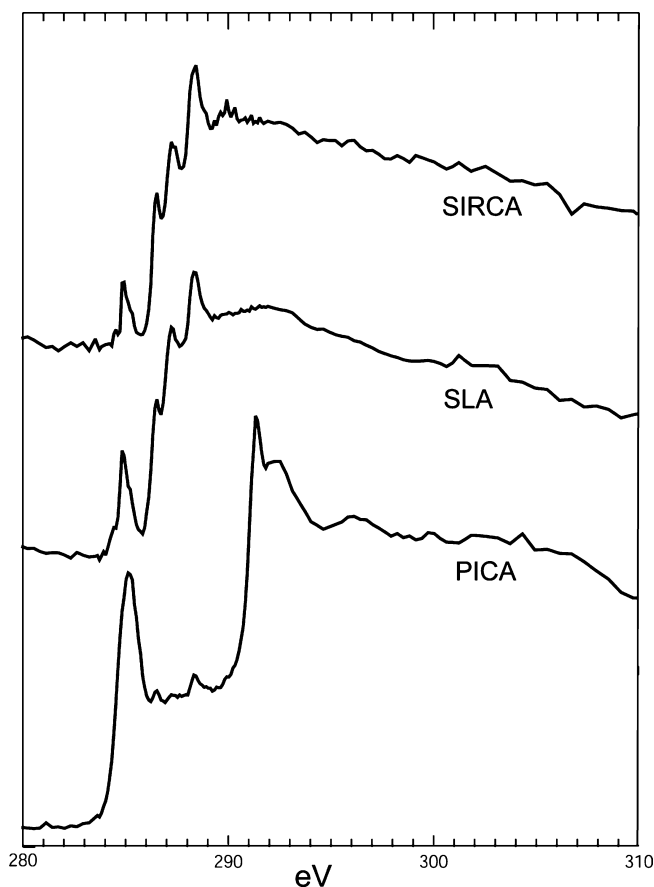

Fig. 12. Carbon XANES spectra taken from preflight samples of the three materials considered for use in the thermal protection system on the Stardust SRC. The forward heatshield was made from PICA and the backshell was made from SLA-561. SIRCA was not ultimately used in the Stardust SRC.

289.8 eV, indicating the presence of a phenolic or methylphenolic functional group associated with the graphite. For comparison, the carbon XANES spectrum from a SIRCA sample (not ultimately used on Stardust) was nearly identical to the carbon XANES spectrum from the SLA sample but with a slight difference in the 290 eV region (Fig. 12).

Infrared Measurements

Mid-IR spectra (4000–650 cm^{-1}) were collected from grain-sized samples of the SRC postflight heatshield and backshell materials using the FTIR ALS beamline. The grains were placed directly on KBr windows and measured in transmission mode without any further sample preparation. Since the SLA used for the SRC backshell consists of a highly filled elastomeric silicone material containing cork as one filler ingredient, it is perhaps not surprising that its overall spectrum has many similarities of other silicon-
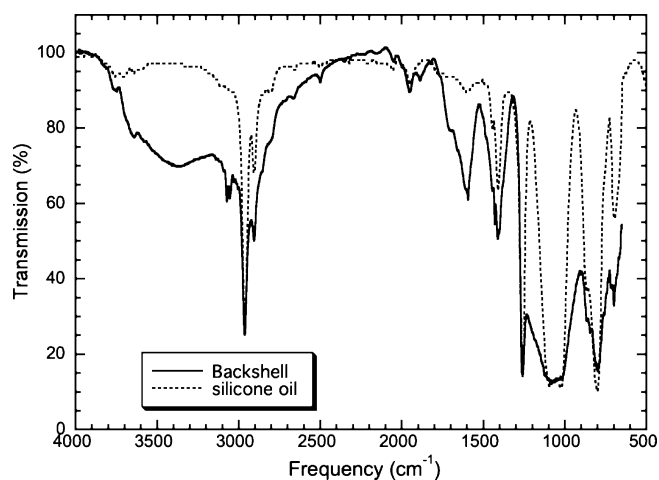
Fig. 13. The 4000–650 cm^{-1} (2.5–15.4 μm) IR spectra of backshell SLA sample E51049 (solid line) compared with the Omnic© library database spectrum of silicone oil (dashed line). The similarities in the spectra are consistent with the presence of Si-bearing organics in both materials.

Fig. 14. Samples were taken from six different locations on the heatshield and backshell for investigation by ultra-L^{2}MS. These include 51043 (heatshield—stagnation point at the nose—PICA), 51044 (heatshield—leading edge of outer rim—PICA), 51047 (heatshield—trailing edge of outer rim—PICA), 51046 (backshell—upper lip with honeycomb support exposed—SLA), 51050 (backshell—outer conical rim—SLA), and 51049 (backshell—RTV sealed penetration on the outer conical rim—SLA).

containing organics like silicone oil (Fig. 13). IR spectra of backshell (SLA) grain (E51049) show strong aliphatic C-H stretching mode bands in the 3000–2800 cm^{-1} region, as well as aromatic C-H stretching mode bands at 3072 and 3054 cm^{-1} (Fig. 13). The dominant C-H stretching feature in this sample does not fall at the location of the -CH$_2$- absorption near 2933 cm^{-1} that is prominent in Stardust aerogel tracks observed to contain excess organics (Sandford et al. 2006; Bajt et al. 2009).

The infrared spectrum of a sample taken from the nose of the forward (PICA) heatshield (E51043) was found to be featureless and is consistent with graphite, a metal, or perhaps metal oxide. The sample looked metallic and crystalline under the optical microscope and showed a dendritic structure.

LC-FD/TOF-MS Measurements

The LC-FD/TOF-MS analysis was used to examine samples of the Stardust heatshield paint edge (E51047; 8.5 mg), heatshield nose (E51043; 0.6 mg), heatshield edge (E51044; 0.2 mg), and backshell (E51049; 0.1 mg). The Stardust heatshield and backshell samples analyzed in this study contained a variety of amino acids and amines including D- and L-aspartic and glutamic acids, D- and L-serine, D- and L-alanine, BALA, GABA, EACA, L-valine, MA, EA, and MEA with total amine concentrations ranging from 930 to 8300 nmol per gram of sample (Table 2). EACA was the most abundant amine in these Stardust samples accounting for 50 to 85% of the total amine concentration. Its most likely source is Nylon-6 contamination from the sample storage containers. The fact that most of these
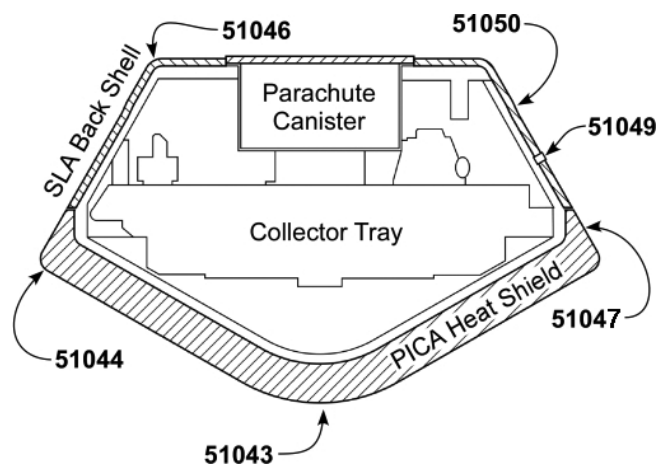
compounds were not detected in the Stardust flight aerogel witness tile (see below) suggests that the Stardust flight aerogel samples were not extensively contaminated with terrestrial amino acids and amines during the Stardust SRC re-entry and landing phases.

Ultra-L^{2}MS Measurements

Samples for investigation by ultra-L^{2}MS were taken shortly after SRC recovery from three different locations on the heatshield and three different locations on the backshell, as indicated in Fig. 14. Acquisition and preparation of these samples are described in more detail in the SOM. For each sample, 50 single-shot spectra were acquired and summed to give the representative mass spectra presented in Figs. 15a and 15b. A difference is readily apparent in both the abundance and distribution of organic species observed between the heatshield samples and those from the backshell. For the heatshield samples, the leading outer conical edge of the heatshield (#51044) showed the greatest profusion of organic species and showed a pronounced enrichment of relatively volatile low-mass hydrocarbons, unlike the samples from the trailing edge (#51047) or stagnation point at the nose (#51043), Particularly prominent is naphthalene (C$_{10}$H$_8$; 128 amu) and its C$_n$-alkylated homologues (i.e., C$_{10}$H$_9$-[CH$_2$]$_n$H; 142, 156, 170, . . . amu), as well as several oxygenated aromatics that are either conspicuously absent or present in greatly diminished abundance in the other
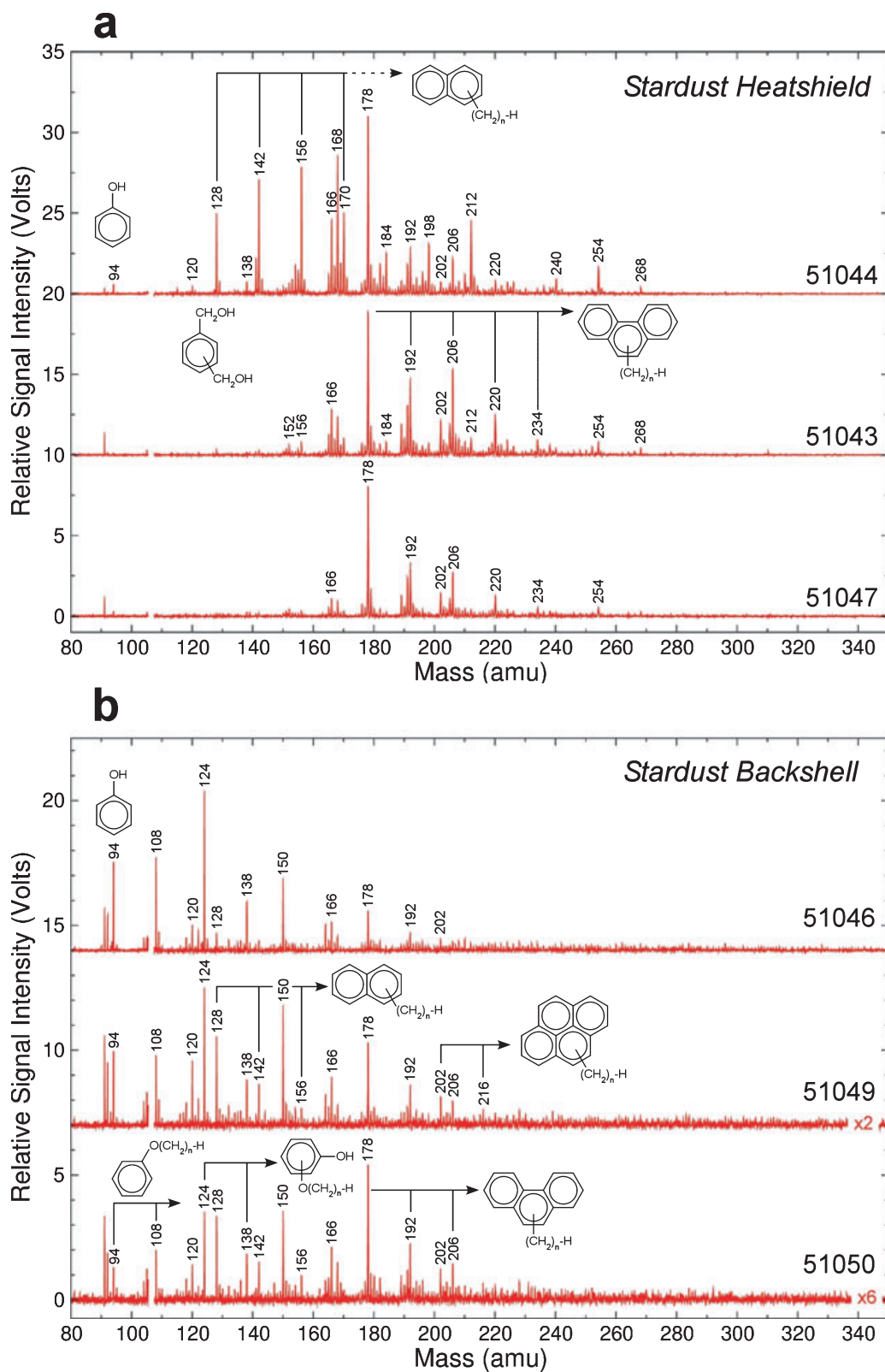
Fig. 15. Mass spectra taken from samples from SRC locations on the a) heatshield and b) backshell as noted in Fig. 14. Species detected include 1–4 ring aromatic species, their C_n-alkylated homologues, oxygenated aromatics, and low mass phenolic aromatics. The abundance and distribution of these organic species varies significantly between samples, but the distributions do not match those of aromatic species found within aerogel impact tracks in the Stardust collector (see text).

heatshield samples. These include phenol (C_6H_5OH; 94 amu) and most likely a dimethoxybenzene isomer ($HOCH_2C_6H_4CH_2OH$; 138 amu) and its C_n-alkylated homologues. It seems likely these oxygenated aromatics represent monomer fragments produced from the pyrolysis of the phenolic resin in the heatshield. The higher mass peaks observed at 240, 254, and 268 amu likely represent the products of gas-phase free radical recombination reactions. For example the 254 amu peak is consistent with the recombination of naphthyl radicals (i.e., $C_{10}H_7 + C_{10}H_7 \rightarrow C_{10}H_7-C_{10}H_7$). The remaining spectra from the trailing edge (#51047) or stagnation point at the nose (#51043) are self-similar and are dominated by the three and four ring aromatics phenanthrene ($C_{14}H_{10}$; 178 amu) and pyrene ($C_{16}H_{10}$; 202 amu) (and associated isomers) along with their C_n-alkylated homologues. The relative lack of oxygenated aromatics may represent a sampling artifact or be indicative of a different thermal environment.

In contrast to the heatshield samples, the three backshell samples all show mass spectra that are dominated by low mass phenolic aromatics that overlay a much weaker distribution of two, three, and four ring fused aromatic species. The concentration of the organic species varies considerably between samples, being most abundant in the upper lip of the SLA (#51046) and least abundant around the outer conical rim of the SLA (#51050). It is unclear whether the greater abundance of oxygenated aromatics in these samples is a consequence of the lower heat flux experience by the backshell (approximately 250 W cm^{-2}) or due to the re-deposition of gas phase species initially liberated from PICA heatshield.

Fortunately, the peak heating during the ablative phase of atmospheric entry happens at high altitudes where pressure equilization results in the intake of very little total air into the SRC. Nonetheless, ablation of the heatshield and backshell during re-entry likely produced volatile aromatic species that could have penetrated into the SRC during pressure equalization. However, even in a worst case scenario this could not account for the range and diversity of organic species observed, for example, by ultra-L^{2}MS along aerogel impact tracks. In particular, there is no evidence in the heatshield and backshell mass spectra for the odd mass aromatic species that have been previously observed and interpreted as evidence for aromatic nitrile species being present in collected cometary dust grains (see Clemett et al. 2010). In this context it is worth noting that while the emission spectra of the plasma formed in the shock front generated by the SRC during re-entry was dominated by CN and $N_2{}^+$ species, we find no evidence for the generation of

N-containing aromatics on either the heatshield or the backshell.

In summary, the heatshield and backshell, and their solid ablation products, have an organic character. The nature of these materials differs significantly from the organics seen in the cometary collector and, to date, there have been no indications that materials associated with the heatshield and backshell and their ablative re-entry into Earth's atmosphere found their way into the sample canister within the SRC.

Sample Canister Filter Contents

The LC-FD/TOF-MS analysis was also used to examine samples taken from the interior of the SRC filter (5208,1,5,1,2). Less than a total of 25 nmol per gram of soluble amines were found in acid hydrolyzed hot water extracts of the filters (Table 2). This suggests that the filter was not called on to remove any significant amount of these materials from the air when the SRC re-pressurized during re-entry. MEA, glycine, and EACA were the most abundant primary amines detected.

Gas Samples Taken during and after SRC Recovery

Several gas samples were taken during and after the recovery of the SRC from its UTTR landing site on January 15, 2006. This was done in an attempt to assess the nature of any gases that may have outgassed from the SRC's thermal protection system and been exposed to the sample canister's inlet filter. Four 1 L samples of air were taken shortly after the SRC Recovery Team arrived at the landing site using pre-evacuated and cleaned Grab Sample Canisters (GSC). By this time the SRC had had sufficient time during its parachute descent and subsequent time on the ground before being located to cool to ambient temperatures. One sample was taken from within 1 cm of the front surface of the heatshield and another was taken at the location of one of the two backshell air inlet vents shortly after the first Recovery Team member arrived at the SRC. A second pair of samples was taken after the remainder of the Recovery Team arrived about 20 min later. After the SRC had been transported back to the temporary cleanroom at the UTTR Avery Complex, three additional 1 L samples were taken—two from near the heatshield and one from near one of the SRC backshell vents. These samples were delivered to the ISO9001:2000 certified Toxicology Laboratory at NASA's Johnson Space Center for analysis on January 18, 2006. In addition, tests were made of the dry N_2 gas being used to purge the cabinet in which the Stardust samples are

stored in the Stardust Cleanroom at JSC. Details of the analysis of these samples can be found in the SOM.

Two categories of compounds were reported: target compounds (multiple level calibration) and nontarget compounds (no calibration-concentration estimated from historical "B" response factors). Isopropanol and 1,1,1,2-tetrafluoroethane concentrations were very high in some GSC samples; therefore the results reported are from a second analysis using a smaller sample volume.

The detailed GC and GC/MS analytical results are reported in ppb in Table S2 in the SOM. Target compounds were identified and reported if their concentration was greater than 1 ppb. If the concentration of a compound was less than 1 ppb, it was labeled as "not detected" (ND). If the concentration was greater than 1 ppb and less than 5 ppb, the compound was labeled as "Trace." An attempt was made to identify nontarget compounds, but compounds with incomplete mass spectra could not be identified with certainty. This type of compound is reported in Table S2, but identification is limited to compound class.

Very little is seen in terms of contaminants, the two main exceptions being isopropanol and 1,1,1,2-tetrafluoroethane, which are seen in a few of the samples. The isopropanol is probably associated with "wet wipes" and the 1,1,1,2-tetrafluoroethane is probably from pressurized "dusters" used to prepare the UTTR clean room. Neither is thought to be of cometary origin and since both are volatile, neither is expected to have significantly compromised the curated samples.

UTTR Soils

The SRC descended on its parachute in a moderate crosswind and first struck the ground more or less directly on the tip of the heatshield's "nose cone," at which time the parachute detached from the SRC. After its initial impact, the SRC bounced several times downwind, striking on the side of the backshell and two locations on the rim. None of the impact sites on the SRC overlapped the two air vents on the backshell. The temporal order of the strikes on the SRC is not certain, but based on the impact marks on the SRC and the size and shape of the depressions in the ground, the last small bounce was clearly on the rim of the SRC. After this last bounce, the SRC ended up on its rim, on which it rolled in a weaving manner downwind for a total of about approximately 20 m. Near the end of the roll, the SRC had slowed enough that several times it flopped down on the side of the backshell briefly before coming back up to roll on the rim a little further. Finally the SRC tipped onto the side of its backshell for good,

Fig. 16. The SRC as it was found upon recovery at the UTTR. The marks on the heatshield resulting from the initial impact on the SRC nose and one of the subsequent impacts on the edge of the SRC can clearly be seen in this picture. Two additional marks not visible in this picture, one on the rim of the heatshield and one on the edge of the backshell, were also apparent. The circle the SRC rolled in before coming to a stop is clearly apparent in the surrounding mud; the slight discoloration is due to small portions of the SRC's thermal ablation materials that adhered to the mud as it rolled.

rolled in almost a complete circle, and came to rest on its side (Fig. 16).

The ancient lakebed in which the SRC landed is composed largely of very fine carbonate muds that are remnants of the Pleistocene Lake Bonneville. The water table is very close to the surface of the lakebed and the ground water contains large concentrations of dissolved salts. As a result, the surface soils contain a variety of evaporates. The soil at the SRC recovery site consisted of a wet, cloying mud that stuck tenaciously to both clothing and gear. No standing water or snow was present at the recovery site. Fortunately, the thermal protection system of the SRC provided an unexpected benefit with regard to the sticking of this mud to the capsule itself. After re-entry, the SRC's surfaces were covered by friable material consisting of ablation products resulting from re-entry of the capsule and the other portions of the heatshield/backshell. This outer layer of material stuck efficiently in the mud. Thus, rather than mud sticking to the capsule, the outermost layers of the capsule were pulled off and remained in the mud. As a result, the SRC came to a stop on its side with almost no mud adhering to it.

During the subsequent recovery process, the SRC was lifted into a special carrier on which it was sealed into doubled bags, and it came into no further contact with local soils. Soil samples were taken at the original landing impact site, the sites of subsequent bounces, and along the roll track. Soil samples were also taken
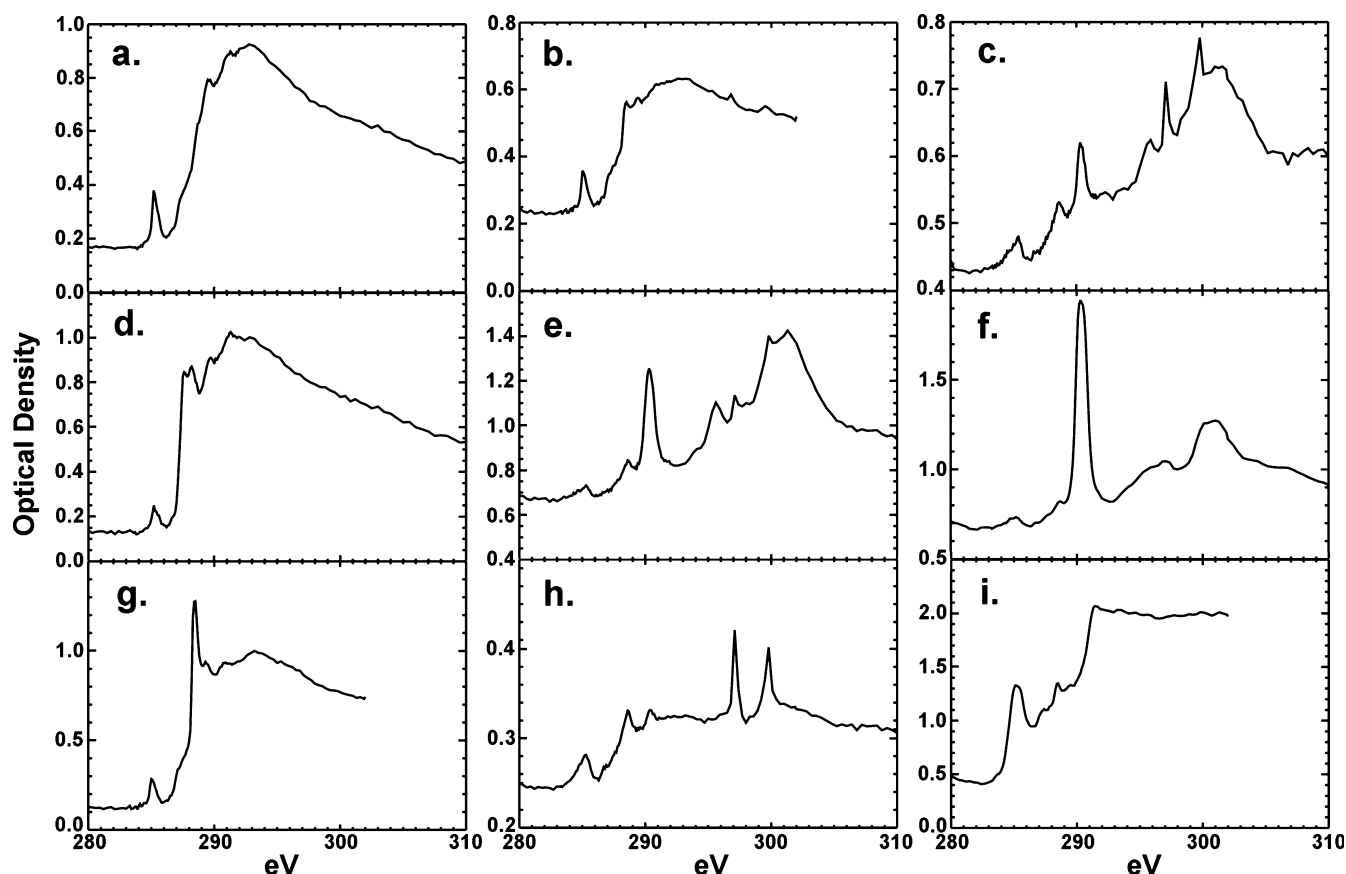
Fig. 17. Carbon XANES spectra of representative grains from UTTR soil sample M5213,3. Panels (a), (b), (c), and (d) contain spectra of organic matter from the soil. Panels c), e), f), and h) show organic features, a carbonate absorption peak at 290.2eV, and potassium absorption peaks at 297.2 and 299.6 eV. Panel i) shows the presence of disordered graphite and is likely from ablated materials shed from the SRC heatshield or backshell.

from directly under the SRC (after it was removed) and from several nearby locations the SRC had not come into contact with. These samples were later examined by members of the Organics PE Team using a variety of analytical techniques.

STXM/XANES

STXM/XANES spectra were collected in the energy range from 280–310 eV on soil samples M4762,5, M4762,6, and M5213,3. These are soil samples collected from impact pits made in the lakebed mud during the SRC's landing. All these samples contained bits of heatshield that could be easily identified visually. Details of the preparation of these samples for analysis can be found in the SOM.

Figure 17 shows plots of the different carbon XANES spectra obtained from soil sample 5213,3 but are representative of all of the soil samples. Panels (a), (b), (d), and (g) contain spectra of organic matter from the soil. The soil samples also contained carbonates

(Figs. 17c, 17e, and 17f), potassium (Figs. 17c and 17h), and several different types of organic carbon. The 2p π* bond energy of carbonates occurs at 290.2 eV (Stohr 1992) and the potassium $L_{2,3}$ edge absorption peak energies occur at 297.2 eV and 299.6 eV (Guan et al. 2005). Some of the carbon XANES spectra in Fig. 17 are similar to those from soil samples reported by Solomon et al. (2007), Courdouan et al. (2007), and Lehmann et al. (2008). We see humic acid substances similar to those they report, although the humic materials in the UTTR soils are spatially closely associated with both the carbonate and potassium (Figs. 17c, 17e, 17f, and 17h). Figure 17g is a typical spectrum one obtains from bacteria (Wirick et al. 2004), and the spectra in Figs. 17a and 17b are similar to standard spectra of lipid biomolecules. The spectrum in Fig. 17d is similar to that of polyethylene. Disordered graphite (Smith and Lobo 2006) was found in some samples (Fig. 17i). The disordered graphite is likely from heatshield material that was altered upon

re-entry and that stuck in the mud when the SRC impacted the ground (compare to the PICA spectrum in Fig. 12).

The C-XANES data from other soil samples (4762,5 and 5213,3) similarly showed the presence of the carbonates calcite, dolomite, aragonite, and also graphite. Again, the graphite is likely associated with heatshield material.

Carbonate-containing sub-micrometer sized particles have been identified in tracks in the Stardust aerogel (Mikouchi et al. 2007; Wirick et al. 2007; Flynn et al. 2008), so the presence of carbonates in soil samples from the landing site raises the concern that the carbonates in the aerogel could be soil contamination. However, a comparison of the C-XANES spectra from the landing site soil samples to C-XANES spectra from carbonate-containing Stardust samples showed no associated organic matter contamination in the Stardust samples from the landing site soils analyzed. We therefore conclude that it is unlikely that these carbonates are due to soil from the landing site getting into the SRC. However, any carbonate materials discovered in the Stardust collection should be considered suspect until possible soil contamination can be reasonably ruled out.

LC-FD/TOF-MS and Soluble Amines

Compared to the SRC heatshield and backshell, the UTTR mud sample analyzed in this study (M4761,2; 109 mg wet weight) contained a much lower abundance of amino acids and amines with a total concentration of 140 nmol per gram (Table 2). In contrast to the heatshield and backshell samples, MA and EA were not detected in the UTTR mud sample above the 0.1 nmol per gram level. The presence of several D-amino acids in the soils, including D-aspartic and glutamic acids, D-serine, and D-alanine, that were not detected in the Stardust flight aerogel witness tile provides additional evidence that the Stardust flight aerogel samples were not extensively contaminated with terrestrial amino acids and amines during the Stardust SRC landing phase.

Microprobe Laser-Desorption Laser-Ionization Mass Spectrometry

Microprobe laser-desorption laser-ionization mass spectrometry analysis of soil from the Stardust SRC landing site revealed no significant presence of PAHs (Spencer and Zare 2006).

Gas Chromatography–Mass Spectrometry

Water-soluble polar nonvolatile organic compounds were identified in the soils by GC-MS. The most abundant were amino acids. The major amino acids were glycine (approximately 61 ppb), D-alanine (approximately 22 ppb), L-alanine (approximately 54 ppb), DL-glutamic (approximately 77 ppb), DL-aspartic, serine, and valine (abundances are qualitative). Ion chromatography (IC) was used to detect the nonvolatile anions formate (13 ppm), acetate (1 ppm), chloride (32ppt) and 72 ppt (sample # M4761,3), and sulfate (32 ppm).

Summary of Potential Contaminants from Flight, Re-Entry, and Recovery of the SRC

The accumulation of local soils (mud) from the recovery site was a major issue of concern for the Stardust Science Team prior to recovery of the SRC. Fortunately, integrity of the SRC during landing, the relative inability of the mud at the recovery site to stick to the SRC, and the fact that none of the bouncing impacts occurred at the locations of the two backshell vents greatly decreased the magnitude of this concern. At present, analyses made using a number of analytical techniques show no indications that soils from the recovery site infiltrated the sample canister or in any way contaminated the returned samples.

CONTAMINATION CONTROL AND ASSESSMENT FOR SAMPLE RETURN MISSIONS—STARDUST LESSONS LEARNED

The small nature of the samples returned by the Stardust spacecraft made it critical that careful attention be paid to the issues of contamination control and assessment. Indeed, sample return missions in general must pay closer attention to these issues than other types of spacecraft missions. To its credit, the Stardust Team recognized this point from the very beginning and carried out a number of activities designed to address this issue (of which this paper is one result). However, the Stardust mission was a very cost-constrained mission and the team had to address issues that had never been thoroughly dealt with before. Reflection on the Stardust effort therefore provides some important "lessons learned" about contamination control and assessment, both for approaches that worked well and for approaches that could be improved. Here, we list a few key points:

1. Efforts need to be made both for contamination control, i.e., to minimize contamination, and contamination assessment. No matter how good contamination control is, there will be some contamination, and it is critical to characterize the nature of the contaminants so they can be distinguished from returned samples. Members of the Stardust Team did their best to carry out such

efforts on a tight schedule and with limited budget, but ideally these activities would be fully integrated into a sample return mission's budget and schedule.

2. Contamination control and assessment requires cooperative efforts be made that involve the spacecraft manufacturers, the spacecraft operators, the mission's Science Team, and the NASA Curatorial Office. Each of these groups should identify an individual or individuals responsible for organizing contamination control and assessment activities, and these individuals need to work closely together across organizational boundaries. Stardust benefited immensely from Science Team members who were willing to devote considerable time and effort to this work, including one Science Team member who was also on the NASA Curatorial staff (coauthor MZ).

3. Oddly enough, one important issue that *everybody* on the mission needs to address early is to agree on what is meant by the word "clean" and how this definition will translate into operational activities. It is surprising how this simple word can mean very different things to different people. For example, a spacecraft engineer may see "clean" as an issue of eliminating surface particulates of a certain size and clean something by wiping it with a solvent soaked wipe, while an organic chemist may flinch in horror at the uniform organic residue left behind when the solvent evaporates. Note that the agreed on definition of "clean" may well differ from mission to mission, depending on the nature of the expected sample and how it will be analyzed.

4. During construction of the spacecraft and sampling system, it is critical to document what components/materials are used. Where possible, samples of these materials should be collected and archived for ultimate storage by the NASA Curatorial Office *at the time of manufacture*. The Stardust Team did some of this, but there were still a number of cases where "standards" of construction components were not available during preliminary examination and could not be acquired 7+ years after the actual assembly of the spacecraft.

5. It is important to use "witness coupons" to track the introduction of contaminates during the manufacture, flight, and recovery of the spacecraft, and during the subsequent removal of the samples from the SRC. These coupons need to be removed and examined quickly so that problems associated with unexpected or problematic contaminants can be dealt with rapidly (again, these activities should be explicitly funded and scheduled within the mission).

6. Witness coupons need to be designed so that they can easily be divided and distributed to multiple analysts. The Stardust witness coupons consisted of single aluminum or sapphire plates, and a single aerogel tile. It proved to be very difficult to examine these coupons by multiple analytic techniques.

7. Sample return spacecraft should carry a significant number of relevant witness coupons. Stardust carried only one small tile of flown, but unexposed, aerogel. This material was a critical standard that many investigators needed for comparison against aerogel tiles that were exposed to the comet. This material represents the all-important "blank" or "control" sample that is critical to the interpretation of many studies of the actual cometary samples. This is particularly important for studies of organics. It would have been very helpful to have more of this kind of material available for Stardust.

8. It is not always clear what materials will work best for contamination control and assessment and different materials can result in different analytical constraints. Thus, where possible, it is generally desirable to use more than one type of witness coupon.

9. Plans must be made in advance so the NASA Curatorial Office is prepared to store and distribute not only the returned samples, but also the associated contamination control and assessment materials (witness coupons, samples of spacecraft materials, etc.).

10. Last, but not least, missions that desire to use silica aerogel as a collector medium should devote additional development effort to the production of the cleanest possible aerogel. The inclusion of stray particulates and the presence of structural carbon within the aerogel significantly complicate the analysis of collected samples. The further development of other types of aerogel (for example, carbon and tantalum aerogels) would also be very useful.

CONCLUSIONS

Numerous sources of potential organic contaminants could have greatly complicated the interpretation of the organic (and inorganic) portions of the samples returned from comet 81P/Wild 2 by the Stardust spacecraft. Studies of controls and the returned samples suggest that most of these potential sources did not contribute any significant material to the collectors.

In particular, contamination from soils at the recovery site and materials associated with the ablation of the heatshield do not appear to be significant problems. In addition, contamination accumulated from the spacecraft environment during flight also does not appear to be a significant problem. The lack of these materials is a testament to the efforts made by the Stardust Team to minimize and control contamination whenever and wherever possible before, during, and after the flight.

The largest source of concern is associated with the carbon present in the original aerogel. This carbon was fortunately not distributed among a complex mixture of organics, but was instead largely present in a few simple forms (mostly as $-CH_3$ groups). However, there does appear to be some variations in this carbon component between and within individual aerogel tiles. In addition, while the initial carbon is dominated by just a few forms, some conversion of this original material into new organic forms appears to happen during particle impact. This issue is particularly problematic for lightweight PAHs. However, in most cases the organics resulting from the impact process do not appear to overwhelm the signature of the returned cometary organics, which can generally be recognized through their different compositions, association with other cometary materials (e.g., minerals), or the presence of isotopically anomalous H and N.

In a few cases, specific molecules appear as common contaminants associated with processing, shipment, or storage of the samples. For example, EACA, [(NH2(CH2)5COOH)], a monomer of the Nylon-6 polymer, is seen in many samples and is likely due to Nylon-6 contamination during storage and shipping.

Overall, these results indicate that contamination issues do not, and will not, preclude the investigation of cometary organics in the samples. Nonetheless, as with any studies of the organics in extraterrestrial materials, extreme caution should continue to be taken to assess the potential impact of organic contaminants when studying any Stardust samples.

Editorial Handling—Dr. Donald Brownlee

REFERENCES

Anderson W. W. and Ahrens T. J. 1994. Physics of interplanetary dust capture via impact into organic polymer foams. *Journal Geophysical Research* 99:2063–2071.

Bajt S., Sandford S. A., Flynn G. J., Matrajt G., Snead C. J., Westphal A. J., and Bradley J. P. 2009. Infrared spectroscopy of Wild 2 particle hypervelocity tracks in Stardust aerogel: Evidence for the presence of volatile organics in cometary dust. *Meteoritics & Planetary Science* 44:471–484.

Bernstein M. P., Sandford S. A., Allamandola L. J., Gillette J. S., Clemett S. J., and Zare R. N. 1999. Ultraviolet irradiation of polycyclic aromatic hydrocarbons (PAHs) in ices: Production of alcohols, quinones, and ethers. *Science* 283:1135–1138.

Brownlee D. E., Tsou P., Anderson J. D., Hanner M. S., Newburn R. L., Sekanina Z., Clark B. C., Hörz F., Zolensky M. E., Kissel J., McDonnell J. A. M., Sandford S. A., and Tuzzolino A. J. 2003. Stardust: Comet and interstellar dust sample return mission. *Journal of Geophysical Research* 108:#E10 8111, pp. 1-1–1-15.

Brownlee D., Tsou P., Aléon J., Alexander C. M. O'D., Araki T., Bajt S., Baratta G. A., Bastien R., Bland P., Bleuet P., Borg J., Bradley J. P., Brearley A., Brenker F., Brennan S., Bridges J. C., Browning N. D., Brucato J. R., Bullock E., Burchell M., Busemann H., Butterworth A., Chaussidon M., Cheuvront A., Chi M., Cintala M. J., Clark B. C., Clemett S. J., Cody G., Colangeli L., Cooper G., Cordier P., Daghlian C., Dai Z., d'Hendecourt L., Djouadi Z., Dominguez G., Duxbury T., Dworkin J. P., Ebel D. S., Economou T. E., Fakra S., Fairey S. A. J., Fallon S., Ferrini G., Ferroir T., Fleckenstein H., Floss C., Flynn G., Franchi I. A., Fries M., Gainsforth Z., Gallien J.-P., Genge M., Gilles M. K., Gillet P., Gilmour J., Glavin D. P., Gounelle M., Grady M. M., Graham G. A., Grant P. G., Green S. F., Grossemy F., Grossman L., Grossman J. N., Guan Y., Hagiya K., Harvey R., Heck P., Herzog G. F., Hoppe P., Hörz F., Huth J., Hutcheon I. D., Ignatyev K., Ishii H., Ito M., Jacob D., Jacobsen C., Jacobsen S., Jones S., Joswiak D., Jurewicz A., Kearsley A., Keller L. P., Khodja H., Kilcoyne A. L. D.,

Kissel J., Krot A., Langenhorst F., Lanzirotti A., Le L., Leshin L. A., Leitner J., Lemelle L., Leroux H., Liu M.-C., Luening K., Lyon I., MacPherson G., Marcus M. A., Marhas K., Marty B., Matrajt G., McKeegan K., Meibom A., Mennella V., Messenger K., Messenger S., Mikouchi T., Mostefaoui S., Nakamura T., Nakano T., Newville M., Nittler L. R., Ohnishi I., Ohsumi K., Okudaira K., Papanastassiou D. A., Palma R., Palumbo M. E., Pepin R. O., Perkins D., Perronnet M., Pianetta P., Rao W., Rietmeijer F. J. M., Robert F., Rost D., Rotundi A., Ryan R., Sandford S. A., Schwandt C. S., See T. H., Schlutter D., Sheffield-Parker J., Simionovici A., Simon S., Sitnitsky I., Snead C., Spencer M. K., Stadermann F. J., Steele A., Stephan T., Stroud R., Susini J., Sutton S. R., Suzuki Y., Taheri M., Taylor S., Teslich N., Tomeoka K., Tomioka N., Toppani A., Trigo-Rodríguez J. M., Troadec D., Tsuchiyama A., Tuzzolino A. J., Tyliszczak T., Uesugi K., Velbel M., Vellenga J., Vicenzi E., Vincze L., Warren J., Weber I., Weisberg M., Westphal A. J., Wirick S., Wooden D., Wopenka B., Wozniakiewicz P., Wright I., Yabuta H., Yano H., Young E. D., Zare R. N., Zega T., Ziegler K., Zimmerman L., Zinner E., and Zolensky M. 2006. Comet 81P/Wild 2 under a microscope. *Science* 314:1711–1716.

Chyba C. F. and McDonald G. D. 1995. The origin of life in the solar system: Current issues. *Annual Review of Earth and Planetary Sciences* 23:215–249.

Chyba C. F. and Sagan C. 1992. Endogenous production, exogenous delivery and impact-shock synthesis of organic molecules: An inventory for the origin of life. *Nature* 355:125–132.

Clemett S. J., Spencer M. K., Sandford S. A., Nakamura-Messenger K., Hörz F., McKay D. S., and Zare R. N. 2010. Complex aromatic hydrocarbons in Stardust samples collected from comet 81P/Wild 2. *Meteoritics & Planetary Science* 45(5). In press.

Cody G. D., Ade H., Alexander C. M. O'D., Araki T., Butterworth A., Fleckenstein H., Flynn G., Gilles M. K., Jacobsen C., Kilcoyne A. L. D., Messenger K., Sandford S. A., Tyliszczak T., Westphal A. J., Wirick S., and Yabuta H. 2008. Quantitative organic and light-element analysis of comet 81P/Wild 2 particles using C-, N-, and O- μ-XANES. *Meteoritics & Planetary Science* 43:353–365.

Courdouan A., Christl I., Meylan S., Wersin P., and Kretzschmar R. 2007. Characterization of dissolved organic matter in anoxic rock extracts and in situ pore water of the Opalinus Clay. *Applied Geology* 22:2926–2939.

Cronin J. R., Pizzarello S., and Cruikshank D. P. 1988. Organic matter in carbonaceous chondrites, planetary satellites, asteroids, and comets. In *Meteorites and the early solar system*, edited by Kerridge J. F. and Matthews M. S. Tucson, AZ: The University of Arizona Press. pp. 819–857.

Dominguez G., Westphal A. J., Jones S. M., and Phillips M. L. F. 2004. Energy loss and impact cratering in aerogels: Theory and experiment. *Icarus* 172:613–624.

Flynn G. J., Bleuet P., Borg J., Bradley J. P., Brenker F. E., Brennan S., Bridges J., Brownlee D. E., Bullock E. S., Burghammer M., Clark B. C., Dai Z. R., Daghlian C. P., Djouadi Z., Fakra S., Ferroir T., Floss C., Franchi I. A., Gainsforth Z., Gallien J.-P., Gillet P., Grant P. G., Graham G. A., Green S. F., Grossemy F., Heck P. R., Herzog G. F., Hoppe P., Hörz F., Huth J., Ignatyev K., Ishii H. A., Janssens K., Joswiak D., Kearsley A. T., Khodja H., Lanzirotti A., Leitner J., Lemelle L., Leroux H., Luening K., MacPherson G. J., Marhas K. K., Marcus M. A., Matrajt G., Nakamura T., Nakamura-Messenger K., Nakano T., Newville M., Papanastassiou D. A., Pianetta P., Rao W., Riekel C., Rietmeijer F. J. M., Rost D., Schwandt C. S., See T. H., Sheffield-Parker J., Simionovici A., Sitnitsky I., Snead C. J., Stadermann F. J., Stephan T., Stroud R. M., Susini J., Suzuki Y., Sutton S. R., Taylor S., Teslich N., Troadec D., Tsou P., Tsuchiyama A., Uesugi K., Vekemans B., Vicenzi E. P., Vincze L., Westphal A. J., Wozniakiewicz P., Zinner E., and Zolensky M. E. 2006. Elemental compositions of comet 81P/Wild 2 samples collected by Stardust. *Science* 314:1731–1735.

Flynn G. J., Leroux H., Tomeoka K., Tomioka N., Ohnishi I., Mikouchi T., Wirick S., Keller L. P., Jacobsen C., and Sandford S. A. 2008. Carbonate in comets: A comparison of comets 1P/Halley, 9P/Temple 1, and 81P/Wild 2 (abstract #1979). 39th Lunar and Planetary Science Conference. CD-ROM.

Glavin D. P., Dworkin J. P., Aubrey A., Botta O., Doty III J. H., Martins Z., and Bada J. L. 2006. Amino acid analyses of Antarctic CM2 meteorites using liquid chromatography-time of flight-mass spectrometry. *Meteoritics & Planetary Science* 41:889–902.

Glavin D. P., Dworkin J. P., and Sandford S. A. 2008. Detection of cometary amines in samples returned by Stardust. *Meteoritics & Planetary Science* 43:399–413.

Guan L., Suenaga K., Shi Z., Gu Z., and Iijima S. 2005. Direct imaging of the alkali metal site in K-doped fullerence peapods. *Physical Review Letters* 94:045502.

Hittle J. D., Calaway M. J., Allton J. H., Warren J. L., Schwarz C. M., and Stansbery E. K. 2006. Genesis spacecraft science canister preliminary inspection and cleaning (abstract #1411). 37th Lunar and Planetary Science Conference. CD-ROM.

Hörz F., Bastien R., Borg J., Bradley J. P., Bridges J. C., Brownlee D. E., Burchell M. J., Chi M., Cintala M. J., Dai Z. R., Djouadi Z., Dominguez G., Economou T. W., Fairey S. A. J., Floss C., Franchi I. A., Graham G. A., Green S. F., Heck P., Hoppe P., Huth J., Ishii H., Kearsley A. T., Kissel J., Leitner J., Leroux H., Marhas K., Messenger K., Schwandt C. S., See T. H., Snead C., Stadermann F. J., Stephan T., Stroud R., Teslich N., Trigo-Rodríguez J. M., Tuzzolino A. J., Troadec D., Tsou P., Warren J., Westphal A., Wozniakiewicz P., Wright I., and Zinner E. 2006. Impact features on Stardust: Implications for comet 81P/Wild 2 dust. *Science* 314:1716–1719.

Huebner W. F. and Boice D. C. 1992. Comets as a possible source of prebiotic molecules. *Origins of Life and Evolution of the Biosphere* 21:299–315.

Jones S. 2007. A method for producing gradient density aerogel. *Journal of Sol-Gel Science and Technology* 44:255–258.

Keller L. P., Bajt S., Baratta G. A., Borg J., Bradley J. P., Brownlee D. E., Busemann H., Brucato J. R., Burchell M., Colangeli L., d'Hendecourt L., Djouadi Z., Ferrini G., Flynn G., Franchi I. A., Fries M., Grady M. M., Graham G. A., Grossemy F., Kearsley A., Matrajt G., Nakamura-Messenger K., Mennella V., Nittler L., Palumbo M. E., Stadermann F. J., Tsou P., Rotundi A., Sandford S. A., Snead C., Steele A., Wooden D., and Zolensky M. 2006. Infrared spectroscopy of comet 81P/Wild 2 samples returned by Stardust. *Science* 314:1728–1731.

Lehmann J., Solomon D., Kinyangi J., Dathe L., Wirick S., and Jacobsen J. 2008. Spatial complexity of soil organic matter forms at nanometer scales. *Nature Geosciences* 1:238–242.

McKeegan K. D., Aléon J., Bradley J., Brownlee D., Busemann H., Butterworth A., Chaussidon M., Fallon S., Floss C., Gilmour J., Gounelle M., Graham G., Guan Y., Heck P. R., Hoppe P., Hutcheon I. D., Huth J., Ishii H., Ito M., Jacobsen S. B., Kearsley A., Leshin L. A., Liu M.-C., Lyon I., Marhas K., Marty B., Matrajt G., Meibom A., Messenger S., Mostefaoui S., Mukhopadhyay S., Nakamura-Messenger K., Nittler L., Palma R., Pepin R. O., Papanastassiou D. A., Robert F., Schlutter D., Snead C. J., Stadermann F. J., Stroud R., Tsou P., Westphal A., Young E. D., Ziegler K., Zimmermann L., and Zinner E. 2006. Isotopic compositions of cometary matter returned by Stardust. *Science* 314:1724–1728.

Mikouchi T., Tachikawa O., Hagiya K., Ohsumi K., Suzuki Y., Uesugi K., Takeuchi A., and Zolensky M. E. 2007. Mineralogy and crystallography of comet 81P/Wild 2 particles (abstract #1946). 38th Lunar and Planetary Science Conference. CD-ROM.

Nishikawa H., Watanabe E., Ito D., Sakurai Y., Nagasawa K., and Ohki Y. 1996. Visible photoluminescence from Si clusters in gamma-irradiated amorphous SiO_2. *Journal of Applied Physics* 80:3513–3517.

Oro J. 1961. Comets and the formation of biochemical compounds on the primitive Earth. *Nature* 190:389–390.

Oro J., Holzer G., and Lazcano-Araujo A. 1980. The contribution of cometary volatiles to the primitive Earth. In *Life sciences and space research. Vol. 18.—Proceedings of the Open Meeting of the Working Group on Space Biology, Bangalore, India, May 29–June 9, 1979. (A80-50051 22-51)* Oxford and Elmsford, NY: Pergamon Press. pp. 67–82.

Pizzarello S., Cooper G. W., and Flynn G. J. 2006. The nature and distribution of the organic material in carbonaceous chondrites and interplanetary dust particles. In *Meteorites and the early solar system II*, edited by Lauretta D. S. and McSween H. Y., Jr. Tucson, AZ: The University of Arizona Press. pp. 625–651.

Rotundi A., Baratta G. A., Borg J., Brucato J. R., Busemann H., Colangeli L., d'Hendecourt L., Djouadi Z., Ferrini G., Franchi I. A., Fries M., Grossemy F., Keller L. P., Mennella V., Nakamura K., Nittler L. R., Palumbo M. E., Sandford S. A., Steele A., and Wopenka B. 2008. Combined micro-Raman, micro-infrared, and field emission scanning electron microscope analyses of comet 81P/Wild 2 particles collected by Stardust. *Meteoritics & Planetary Science* 43:367–397.

Sandford S. A. and Brownlee D. E. 2007. Response to comment on "Organics captured from comet 81P/Wild 2 by the Stardust spacecraft." *Science* 317:1682.

Sandford S. A., Bernstein M. P., Allamandola L. J., Gillette J. S., and Zare R. N. 2000. Deuterium enrichment of PAHs by photochemically induced exchange with deuterium-rich cosmic ices. *The Astrophysical Journal* 538:691–697.

Sandford S. A., Bernstein M. P., and Dworkin J. P. 2001. Assessment of the interstellar processes leading to deuterium enrichment in meteoritic organics. *Meteoritics & Planetary Science* 36:1117–1133.

Sandford S. A., Aléon J., Alexander C. M. O'D., Araki T., Bajt S., Baratta G. A., Borg J., Bradley J. P., Brownlee D. E., Brucato J. R., Burchell M. J., Busemann H.,

Butterworth A., Clemett S. J., Cody G., Colangeli L., Cooper G., d'Hendecourt L., Djouadi Z., Dworkin J. P., Ferrini G., Fleckenstein H., Flynn G. J., Franchi I. A., Fries M., Gilles M. K., Glavin D. P., Gounelle M., Grossemy F., Jacobsen C., Keller L. P., Kilcoyne A. L. D., Leitner J., Matrajt G., Meibom A., Mennella V., Mostefaoui S., Nittler L. R., Palumbo M. E., Papanastassiou D. A., Robert F., Rotundi A., Snead C. J., Spencer M. K., Stadermann F. J., Steele A., Stephan T., Tsou P., Tyliszczak T., Westphal A. J., Wirick S., Wopenka B., Yabuta H., Zare R. N., and Zolensky M. E. 2006. Organics captured from comet 81P/Wild 2 by the Stardust spacecraft. *Science* 314:1720–1724.

Smith M. A. and Lobo R. F. 2006. The local and surface structure of ordered mesoporous carbons from nitrogen sorption, NEXAFS and synchrotron radiation studies. *Microporous and Mesoporous Materials* 92:81–93.

Solomon D., Lehmann J., Kinyangi J., Amelung W., Lobe I., Pell A., Riha S., Ngoze S., and Verchot L. 2007. Long-term impacts of anthropogenic perturbations on dynamics and speciation of organic carbon in tropical forest and subtropical grassland ecosystems. *Global Change Biology* 14:27–47.

Spencer M. K. 2008. Laser mass spectrometric detection of terrestrial and extraterrestrial polycyclic aromatic hydrocarbons. Ph.D. thesis, Stanford University, Stanford, California, USA.

Spencer M. K. and Zare R. N. 2006. μmL2MS analysis of standards in preparation for the return of NASA Stardust (abstract #1432). 37th Lunar and Planetary Science Conference. CD-ROM.

Spencer M. K. and Zare R. N. 2007. Comment on "Organics captured from comet 81P/Wild 2 by the Stardust spacecraft." *Science* 317:1680.

Spencer M. K., Hammond M. R., and Zare R. N. 2008. Laser mass spectrometric detection of extraterrestrial aromatic molecules: Mini-review and examination of pulsed heating effects. *Proceedings of the National Academy of Sciences* 105:18,096–18,101.

Spencer M. K., Clemett S. J., Sandford S. A., McKay D. S., and Zare R. N. 2009. Organic compound alteration during hypervelocity collection of carbonaceous materials in aerogel. *Meteoritics & Planetary Science* 44:15–24.

Stephan T., Rost D., Vicenzi E. P., Bullock E. S., MacPherson G. J., Westphal A. J., Snead C. J., Flynn G. J., Sandford S. A., and Zolensky M. E. 2008. TOF-SIMS analysis of cometary matter in Stardust aerogel tracks. *Meteoritics & Planetary Science* 43:233–246.

Stohr J. 1992. *NEXAFS spectroscopy*. Springer Series in Surface Sciences, vol. 25. New York, NY: Springer-Verlag.

Tillotson T. M. and Hrubesh L. W. 1992. Transparent ultralow-density silica aerogels prepared by a two-step sol-gel process. *Journal of Non-Crystalline Solids* 145:44–50.

Tsou P., Brownlee D. E., Sandford S. A., Hörz F., and Zolensky M. E. 2003. Wild 2 and interstellar sample collection and Earth return. *Journal of Geophysical Research* 108, #E10, 8113: pp. 3-1 to 3-21.

Westphal A. J., Snead C., Butterworth A., Graham G. A., Bradley J. P., Bajt S., Grant P. G., Bench G., Brennan S., and Pianetta P. 2004. Aerogel keystones: Extraction of complete hypervelocity impact events from aerogel collectors. *Meteoritics & Planetary Science* 39:1375–1386.

Westphal A. J., Bastien R. K., Borg J., Bridges J., Brownlee D. E., Burchell M. J., Cheng A. F., Clark B. C., Djouadi Z., Floss C., Franchi I., Gainsforth Z., Graham G., Green S. F., Heck P. R., Horanyi M., Hoppe P., Hörz F. P., Huth J., Kearsley A., Leroux H., Marhas K., Nakamura-Messenger K., Sandford S. A., See T. H., Stadermann F. J., Teslich N. E., Tsitrin S., Warren J. L., Wozniakiewicz P. J., and Zolensky M. E. 2008. Discovery of non-random spatial distribution of impacts in the Stardust cometary collector. *Meteoritics & Planetary Science* 43:415–429.

Wirick S., Flynn G. J., Keller L., and Jacobsen C. 2004. Evidence for terrestrial organic contamination of the Tagish Lake meteorite (abstract #1532). 35th Lunar and Planetary Science Conference. CD-ROM.

Wirick S., Leroux H., Tomeoka K., Zolensky M. E., Flynn G. J., Tyliszczak T., Butterworth A., Tomioka N., Ohnishi I., Nakamura-Messenger K., Sandford S., Keller L., and Jacobsen C. 2007. Carbonates found in Stardust aerogel tracks (abstract #1534). 38th Lunar and Planetary Science Conference. CD-ROM.

Zolensky M. E., Zega T. J., Yano H., Wirick S., Westphal A. J., Weisberg M. K., Weber I., Warren J. L., Velbel M. A., Tsuchiyama A., Tsou P., Toppani A., Tomioka N., Tomeoka K., Teslich N., Taheri M., Susini J., Stroud R., Stephan T., Stadermann F. J., Snead C. J., Simon S. B., Simionovici A., See T. H., Robert F., Rietmeijer F. J. M., Rao W., Perronnet M. C., Papanastassiou D. A., Okudaira K., Ohsumi K., Ohnishi I., Nakamura-Messenger K., Nakamura T., Mostefaoui S., Mikouchi T., Meibom A., Matrajt G., Marcus M. A., Leroux H., Lemelle L., Le L., Lanzirotti A., Langenhorst F., Krot A. N., Keller L. P., Kearsley A. T., Joswiak D., Jacob D., Ishii H., Harvey R., Hagiya K., Grossman L., Grossman J. N., Graham G. A., Gounelle M., Gillet P., Genge M. J., Flynn G., Ferroir T., Fallon S., Ebel D. S., Dai Z. R., Cordier P., Clark B., Chi M., Butterworth A. L., Brownlee D. E., Bridges J. C., Brennan S., Brearley A., Bradley J. P., Bleuet P., Bland P. A., and Bastien R. 2006. Mineralogy and petrology of comet 81P/Wild 2 nucleus samples. *Science* 314:1735–1739.

SUPPORTING INFORMATION

Additional supporting information may be found in the online version of this article:

Table S1. Comet tray aerogel tiles, batches, and relative luminescence intensities.

Table S2. Analytical results of Stardust air samples.

Please note: Wiley-Blackwell are not responsible for the content or functionality of any supporting materials supplied by the authors. Any queries (other than missing material) should be directed to the corresponding author for the article.